Czech University of Life Sciences Prague
Faculty of Environmental Sciences

DIPLOMA THESIS

Prediction System for Soil Water Pressure Head

Arij Chmeis

Department of Water Resources and Environmental Modeling

Supervisor of the diploma thesis: doc. Ing. Michal Kuráž, Ph.D.
Study programme: Landscape Engineering
Field of study: Environmental Modeling

Prague, 2021

CZECH UNIVERSITY OF LIFE SCIENCES PRAGUE

Faculty of Environmental Sciences

DIPLOMA THESIS ASSIGNMENT

Arij Chmeis

Landscape Engineering
Environmental Modelling

Thesis title

Prediction System for Soil Water Pressure Head

Objectives of thesis

Examining evaporation process in an arid vineyard in order to: A. Estimate losses using coupled water, vapor, and heat flow model with automated input to solve the surface energy balance equation, and B. Create a pressure head-prediction scheme using sensors provided by cooperating company Lesprojekt.

Methodology

- Creating a communication protocol with sensors from cooperating company.
- Creating a communication protocol with weather-forecast server.
- Estimating and manually optimizing input parameters.
- Creating an automated input tool for the surface energy balance equation-solution.
- Running DRUtES model using the configuration files with automated input.

The proposed extent of the thesis

60 pages and source code

Keywords

water content, Richards equation, evaporation modeling

Recommended information sources

James Brinkhoff, John Hornbuckle, Carlos Ballester Lurbe, Soil moisture forecasting for irrigation recommendation, IFAC-PapersOnLine, Volume 52, Issue 30, 2019, Pages 385-390, ISSN 2405-8963, https://doi.org/10.1016/j.ifacol.2019.12.586.

Liu, H., Xie, D. & Wu, W. Soil water content forecasting by ANN and SVM hybrid architecture. Environ Monit Assess 143, 187 (2008). https://doi.org/10.1007/s10661-007-9967-9

M. Kuraz, J.R. Bloecher, Hydrodynamics in porous media, CULS in Prague lecture notes, Prague 2020

Expected date of thesis defence

2020/21 SS – FES

The Diploma Thesis Supervisor

doc. Ing. Michal Kuráž, Ph.D.

Supervising department

Department of Water Resources and Environmental Modeling

Advisor of thesis

Ing. Johanna Ruth Blöcher

Electronic approval: 17. 3. 2021

prof. Ing. Martin Hanel, Ph.D.

Head of department

Electronic approval: 17. 3. 2021

prof. RNDr. Vladimír Bejček, CSc.

Dean

Prague on 27. 03. 2021

Author's Declaration

I hereby declare that I carried out this submitted diploma thesis *Prediction System for Soil Water Pressure Head* independently, and only sources listed in the Bibliography were used.

Prague, 30^{th} March 2021 ..... Arij Chmeis

Acknowledgement

I would like to express my sincere gratitude to my supervisor doc. Ing. Michal Kuráž, Ph.D. Thank you for all your guidance and your effort to expand my knowledge and understanding. I would also like to thank Ing. Johanna Blöcher, my advisor, your support and kindness are beyond appreciated. A heartfelt thank you for all the time and energy you extended to help me succeed.

To my wonderful family; my parents, my number one inspiration in life, and my amazing sisters who always believed in me, thank you for all the love you surround me with. I couldn't have made it if it weren't for you.

Thank you to my awesome friends in Prague, for always having my back, for being my second family and making it truly feel like home.

And finally to my partner, Lujayn Layka, thank you for being my rock and my best friend, for cheering me on and inspiring me to never give up. Thank you for your incredible faith in me, for giving me strength, and supporting me through all the tough times. I wouldn't be here without you.

Abstract

Water resources in arid regions around the world are under a lot of strain due to extremely low precipitation rates and very high evaporation. In addition to water scarcity, irrigation methods can be quite inefficient. For example, over-irrigation beyond soil saturation can cause many problems, such as increase in soil salinity and decrease in productive soil capacity.

This research aimed to investigate evaporation losses in a vineyard in San Juan province, Argentina. Trucks are used to deliver irrigation water to the raisin-producing vineyard, which ends up being over-flooded due to poor irrigation schedules, making the process highly costly. For the estimation of evaporation losses, I employed a coupled water, vapor, and heat flow model implemented in DRUtES software (Kuraz, Mayer, and Blöcher, 2020). The model's top boundary condition solves the surface energy balance. For this purpose, solar radiation is needed as an input, which I computed based on equations suggested in the FAO Irrigation and Drainage guideline (Allen et al., 1998) as well as by Saito et al. (2006).

Due to the lack of measurement data on the study site, soil hydraulic and thermal properties were estimated. While climatic data is available from a nearby meteorological station, access to backdated files is not possible. This limited the choice of simulation period. To solve this issue, I created Python codes that produce automated daily procedures to access the weather servers. This transcribed data record is then used as an input for DRUtES configuration files. Communication with sensors that are installed in the soil was also establish using Python-script automation, in order to rectify missing measurements and use them as the model's initial conditions.

The results formed an output record that predicts temperature and pressure head distribution across the study site over the simulated period. A flow-describing system is presented, which allows the calculation of evaporation rate changes with time. The model's estimation of pressure head and soil temperature compares well with the values measured by in-situ soil sensors. The system can be used as a helpful decision-making tool for farmers, in order to optimize the

irrigation process according to the soil and plant needs. This diploma thesis contributed to the ongoing AgriClima (2019) project. The project's objective is to optimize agricultural water-management by applying experience from the Czech Republic to new users in Argentina.

Keywords: Evaporation modelling, Evaporation in vineyards, Richards equation, Water content, Automation tools, Pressure head prediction.

Contents

List of Figures

List of Tables

Chapter 1

Introduction

Currently, it is estimated that water supply is limited in around half of the land surface of our planet. This estimate is only presumed to rise as the food demand increases and thus water resources suffer greater strain (Kool et al., 2014). Evaporation is one of the biggest elements in the composition of any water system, and studying evaporation rates is vital in numerous engineering fields (McMahon et al., 2013). But aside from its applications in industrial areas dealing with heat and moisture transport, evaporation modelling is especially crucial in the understanding of water and energy environmental balance in dry areas. In some regions, agriculture may consume up to 80% of the limited water budget. Increasing the efficiency of water usage by only 10% would translate to 40% more water in those arid areas (Tezza et al., 2019). Since evaporation is a major component of the movement of soil moisture in porous media, better knowledge of its dynamics is imperative for improving water management.

Modelling evaporation is one of the most challenging tasks in the study of coupled water and heat transport systems. It requires thorough examination of the interactions between temperature and pressure head gradients, as well as the significant role the water vapor flux plays in both mass and energy balances (Cahill and Parlange, 1998). Nonetheless, progress in the modelling of evaporation can bring huge benefits particularly for farmers of arid lands. Not only is water an expensive resource for those farmers, but the dryness of soil that is caused by evaporation can leave it extremely hard and insusceptible to irrigation water. By decreasing those harmful effects, workers in the agricultural sector can increase their water-usage efficiency and optimize the quality of their crops.

1.1 Motivation and Goals

The main motivation of this thesis is to develop a prediction system for the pressure head and soil temperature of a commercial vineyard soil, by examining evaporation losses using a numerical coupled liquid water, water vapor, and heat flow model. This mathematical model was built as an extension to the open-source objective library DRUtES during the first year of the AgriClima (2019) project.

The second goal of this research is automating the input to the configuration files of DRUtES. For this task, a Python program was created to estimate actual shortwave radiation and construct a data record to be used in the solution of the surface energy balance equation assigned as the model's boundary condition. Further aims includ the automation of generating an observation measurement file in Python code to be used for model evaluation and validation purposes.

Lastly, the previous objectives are used in characterizing evaporation in a case study site located in San Juan province in Argentina. The resulting estimations comprise a field description that can act as an aiding tool for farmers, and help the agricultural industry in the efforts to improve water-use efficiency in the future.

1.2 Thesis Structure

The second Chapter of this thesis starts with preliminary concepts to introduce definitions and historical theories of evaporation, followed by a description of coupled water, vapor, and heat flows, and their equations and modelling methods. Chapter 2 also details the description of the mathematical model used to simulate the evaporation process, including constitutive relations and the system's implemented boundary conditions. In the third chapter, the structure of methods developed for the computation of the surface energy balance equation as a part of the model's configuration files is presented. The case study used to evaluate the model's performance is also described in this chapter. Chapter 4 contains the results produced by this research, with their subsequent comprehensive analysis explained in Chapter 5. Lastly, Chapter 6 is dedicated to the conclusive findings of this thesis along with recommendations for future research.

Chapter 2

Literature Review

2.1 Evaporation in Soil Science

The evaporation phenomenon is defined as the process where a liquid or solid form of a substance transitions into a vapor form (Brutsaert, 2013). Soil water evaporation (E) poses threats of substancial water loss along with soil salinity. In Kool et al. (2014), authors remark that evaporation from the soil surface makes up between 20-40% of the reported evapotranspiration (ET). Evapotranspirationg is the sum of water evaporation and transpiration from a surface area to the atmosphere. ET comprises more than 95% of the water budget in water-restricted areas. World-wide, ET falls at 60% of precipitation, while evaporation accounts for around 25% of solar energy consumption (Or et al., 2013).

2.1.1 Important definitions

Potential evaporation is the amount of evaporation that would ensue from a saturated surface, given constant surface temperature and atmospheric conditions . This implies that potential evaporation is the evaporative demand of the atmosphere, indicating a maximum value of evaporation. *Actual evaporation*, a value lower than potential evaporation, and is described as the amount of water that is transmitted from a surface into the atmosphere in the form of water vapor (McMahon et al., 2013).

2.1.2 Evaporation phases

Han and Zhou (2013) analysed the evolution of bare soil water evaporation during a constant drying event by laboratory and numerical experiments. Their results showed that the evaporation process can be categorized into three stages:

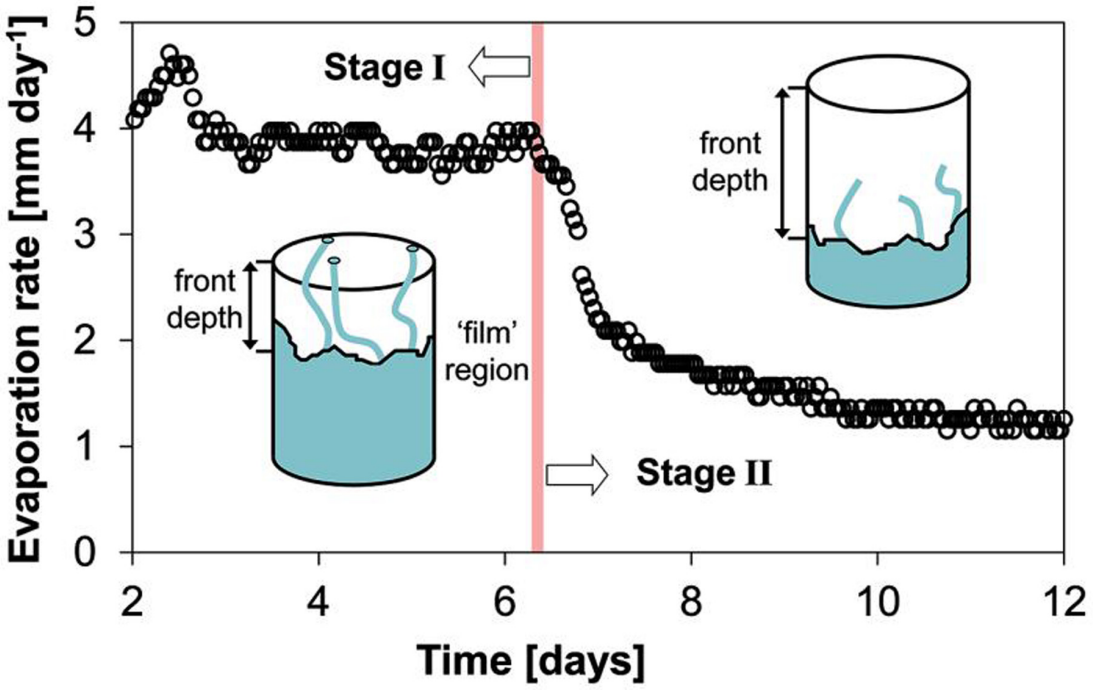

Figure 2.1: Stage I and Stage II of evaporation: Soil is at saturation state in stage I and dries out in stage II, as depicted in Or et al. (2013).

- The first stage: A very short phase, where the peak of evaporation is at soil surface, and is at a high rate (which equals potential evaporation).
- The second stage: The rate of stage II is lower, and the peak and top boundary layer is at subsurface. A dry surface layer starts to appear above evaporation zone and increases in width.
- The third stage: Where the evaporation rate is very low and constant, with the width of the dry surface layer at a constant value as well.

Stage II and III are often coined together, as seen in Figure 2.1 depicting evaporation stages. During stage I, the evaporation rate rapidly increases in the beginning, and then falls almost constant afterwards, then resumes decreasing again in stage II. Or et al. (2013) term the first stage as the *constant rate period*, or CRP, while referring to the second as FRP or the *falling rate period*.

2.1.3 Background theory and methods

Evaporation has been estimated in many ways over the past years. The main methods can be categorized into the following approaches (Burt et al., 2005):

- Water balance method.
- Energy balance method.

- Coupled water and energy balance methods.
- Semi-empirical and empirical methods.

Water-balance method

Generally, evaporation from the soil can be expressed as:

$$E + T = P + I + \Delta S - D - R, \tag{2.1}$$

where E [mm.day^{-1}] and T [mm.day^{-1}] are the evaporation and transpiration respectively, P [mm.day^{-1}] is the precipitation, I [mm.day^{-1}] the irrigation, ΔS [mm.day^{-1}] the change in soil water storage, D [mm.day^{-1}] the drainage losses, and R [mm.day^{-1}] the runoff losses (Burt et al., 2005).

Energy-balance method

The general equation of surface energy balance is expressed as:

$$LE = R_N - G - H, \tag{2.2}$$

where LE [W.m^{-2}] is the outgoing latent heat flux, R_N [W.m^{-2}] is the incoming net solar radiation, G [W.m^{-2}] is the soil heat flux, and H [W.m^{-2}] is the sensible heat flux.
Among the most widely-used models in this category are the Penman and Penman-Monteith methods. These models determine a reference crop ET based on a concept that employs weather variables such as wind speed, relative humidity, air temperature and solar radiation.

The complexity, parameter-sensitivity and requirements of coupled water and energy balance methods contribute to their impracticality and unpopularity in larger researches. Among semi-empirical and empirical methods is the two-stage model where stage I evaporation is limited by energy input solely (Ritchie, 1972). These methods however, are only applicable in bare soil areas.

2.1.4 Parameterization of evaporation

Evaporation rates are difficult to measure directly from the soil. As such, indirect methods like the Bowen ratio-energy balance, or the eddy covariance have almost been the only alternative ways to obtain them (Sakai et al., 2011). The calculation of evaporation rates using numerical models for the coupled water and heat flow transport is indeed possible (Saito et al., 2006). However, despite that fact,

describing thermal and hydraulic soil properties of numerical models remains a challenging task. Evaporation rates are influenced by many factors. Among those are surface soil wetness, atmospheric conditions, and moisture transport in the soil layer. In Kondo et al. (1990), the authors present an evaporation model that describes surface moisture availability as a general expression. They conclude that it is affected by wind velocity, volumetric soil moisture and the ratio of specific air humidity to specific humidity of the saturation value at soil surface temperature. The study also states that substituting the humidity of air adjacent to water in the soil pore for the land surface humidity is only valid in saturated soils.

2.2 Liquid Water, Water Vapor and Heat Flow

Transport of water in bare field soil was analyzed by Cahill and Parlange (1998), where the authors indicated the significant role that the vapor flux plays in the movement of moisture, stating that water vapor flux makes up 10-30% of the total moisture flux. On the other hand, they found that the heat flux caused by vapor transport comprises 40-60 % of the total heat flux. Latent heat-transport carried out by the vapor flux is the most influential process that governs the water-heat coupling (Bittelli et al., 2008). Water vapor diffusion leads to the transfer of latent and sensible heat, thus accounting for a major transport of latent energy due to the evaporation and condensation processes. This is why evaporation cannot be considered isothermal. Neglecting the effect of vapor transfer on the movement of energy may lead to substantial underestimation of soil temperatures. The coupled interactions between liquid water, water vapor and heat flux has been widely recognized as early as 1954. However, despite the proven significance of water vapor in the estimation of surface evaporation, it is still seldom accounted for or calculated in many of the existing evaporation models. Most evaporation modelling neglect the effects of the vapor flux, or the influence of heat transport on water flow, or sometimes even both (Saito et al., 2006).

2.2.1 Richard's equation

Many evaporation models are essentially based on Richard's equation, a nonlinear partial differential equation attributed to L.A. Richards who developed it in 1931, which describes Darcian flow in a variably saturated porous medium (Kuraz, Mayer, and Pech, 2014). In terms of models describing water transport and water/energy exchanges within the land-atmosphere environment, it is considered the most commonly used concept (Vanderborght et al., 2017). Richard's equation

is based on Darcy's law for groundwater flow, and is expressed as:

$$\frac{\partial \theta}{\partial t} = -K \nabla h, \tag{2.3}$$

where K [m.s^{-1}] is the hydraulic conductivity, h [m] is the matric head induced by capillary action, z [m] is the elevation above a vertical datum, and θ [-] is the volumetric water content, (Richards, 1931).

To identify the uniform flux boundary condition that is used in Richard's equation, a surface energy balance solution must be obtained. This condition changes into a pressure-head upon reaching the so-called *critical pressure head*, a threshold that indicates the soil has completely dried out (Vanderborght et al., 2017). Many scientist and researchers have investigated the Richard's equation problem, analysing it (e.g Kačur, 2001) and suggesting different methods for its numerical treatment (e.g Kuraz, Mayer, and Pech, 2014).

2.2.2 Applications of coupled modelling

Authors Saito et al. (2006) built a numerical model that solves the coupled equations of liquid water, water vapor, and heat transport, along with the surface water and energy balance. Irrigation, evaporation, surface precipitation and heat fluxes were considered boundary conditions for liquid water, water vapor, and heat flows. The liquid and vapor phases of water in the soil pores were assumed to be in equilibrium, and soil surface resistance to water vapor flow was neglected. In the heat transport module, the movement of soil heat was considered to occur by conduction, the convection of sensible heat by liquid water flow, and the transfer of latent and sensible heat by diffusion of water vapor. Finite element method and finite differences method were used for spatial and temporal discretizations respectively. This model was able to accommodate different forms of meteorological data and use it in solving the surface energy balance.

In Bittelli et al. (2008), authors use the previous model of non-isothermal solution of the vapor flux equation that considers phase changes and thermally-driven water vapor transport and describe it as:

$$q_v^* = q_v^i + q_v^T, \tag{2.4}$$

where q_v^i is the isothermal vapor flow, and q_v^T is the non-isothermal vapor flow. This implementation demonstrated the importance of vapor transport in energy and soil mass transfer. It also showed the strong influence of temperature variations in soil water dynamics.

Numerical simulations of coupled water, vapor, and heat flow model were employed by Iden et al. (2019) to specify the accuracy of simplified evaporation method (SEM). Authors built a numerical example that simulates a range of soils and lab conditions. These were then used to test the biases of assumptions made in SEM, and investigate the role that the coupled transport plays.

2.3 Mathematical Model

This chapter explains the mathematical model that was derived and implemented in the open-software DRUtES, created by Kuraz, Mayer, and Blöcher (2020). Modelling evaporation is based on the incorporation of both hydrodynamic and thermodynamic processes to obtain an accurate description of flow in porous media.

2.3.1 Hydro-dynamical model

Mathematical description of transport in porous media relies on Darcy's approach to quantify the properties of volume fluxes on a macroscopic scale, instead of from complicated microscopic pathways (Kuráž and Bloecher, 2017). The standard law of mass conservation combined with Darcy's law is expressed as:

$$\frac{\partial \theta}{\partial t} = -\boldsymbol{\nabla} \cdot \vec{q} - S_w, \tag{2.5}$$

where θ [-] is the water content, $\vec{q}$ [m.s^{-1}] are the volume fluxes, and S_w [s^{-1}] refers to the root water uptake term. Modelling of evaporation includes description of couple liquid water, water vapor and heat flows. Thus, when formulated to indicate these components the previous equation becomes:

$$\frac{\partial (\theta_l + \theta_v)}{\partial t} = -\boldsymbol{\nabla} \cdot \vec{q}_l - \boldsymbol{\nabla} \cdot \vec{q}_v - S_w, \tag{2.6}$$

where $theta_l$, $theta_v$ [-] are the liquid and vapore water contents, and $\vec{q}_l$ and $\vec{q}_v$ [m.s^{-1}] are the liquid water flow and water vapor flow respectively. Philip and De Vries (1957) expressed liquid water flow in porous media with thermodynamic conditions as:

$$\vec{q}_l = -K_{lh} \nabla H - K_{lT} \nabla T, \tag{2.7}$$

where K_{lh} [m.s^{-1}] is the hydraulic conductivity, H [m] is the hydraulic head (the sum of pressure head h and geodetic head z), K_{lT} [m^2.K^{-1}.s^{-1}] is the hydraulic/thermodynamic conductivity and T [°C] is the temperature. Water vapor

flow is also formulated in Philip and De Vries (1957) and is given as:

$$\vec{q_v} = -K_{vh}\nabla h - K_{vT}\nabla T, \tag{2.8}$$

where K_{vh} [m.s^{-1}] is the hydraulic conductivity for vapor and K_{vT} [m^2.K^{-1}.s^{-1}] is the hydraulic/thermodynamic conductivity for vapor. By combining equation (2.5) with (2.7) and (2.8) we can express the governing hydro-dynamical equation as (Sakai et al., 2011):

$$\frac{\partial \theta_l}{\partial t} + \frac{\partial \theta_v}{\partial t} = \boldsymbol{\nabla} \cdot (K_{lh} + K_{vh})\nabla h + \frac{\partial K_{lh}}{\partial z} + \boldsymbol{\nabla} \cdot (K_{lT} + K_{vT})\nabla T - S_w. \tag{2.9}$$

2.3.2 Thermodynamical model

Applying heat flow-denotations to the law of mass conservation can be presented as:

$$\frac{\partial Q_h}{\partial t} = -\boldsymbol{\nabla} \cdot \vec{q}_T - S_h, \tag{2.10}$$

where Q_h [J.m^{-3}] refers to the heat energy, q_T [J.m^{-2}.s^{-1}] is the heat flux, and S_h [J.m^{-3}.s^{-1}] refers to the heat source/sink term. The total heat energy is made up of the heat energy of four different components: the solid phase, the liquid phase, the vapor phase and the production/consumption of latent heat due to phase changes. This is expressed as:

$$Q_h = C_s T(1 - \theta_s) + C_l T\theta_l + C_v T\theta_v + L_0\theta_v, \tag{2.11}$$

where C_s, C_l and C_v [J.m^{-3}.K^{-1}] are the specific volumetric heat capacities of solid, liquid and vapor phases respectively, and L_0 [J.m^{-3}] refers to the volumetric latent heat of vaporization. De Vries (1958) remarks that the heat flux is made up of the total sum of the sensible heat of convection by liquid water and water vapor, the latent heat by vapor flow, and the sensible heat conduction described by Fourier's law:

$$q_T = -\lambda(\theta_l)\nabla T + C_l T\vec{q_l} + C_v T\vec{q_v} + L_0\vec{q_v}, \tag{2.12}$$

where $\lambda(\theta_l)$ [J.m^{-1}.s^{-1}.K^{-1}] is the apparent thermal conductivity of soil. By combining equation (2.10) with (2.11) and (2.12) we can express the governing

Thermodynamical equation as:

$$(C_s(1-\theta_s)+C_l\theta_l+C_v\theta_v)\frac{\partial T}{\partial t}+L_0\frac{\partial \theta_v}{\partial t}=\boldsymbol{\nabla}\cdot\lambda(\theta_l)\nabla T- \\ \boldsymbol{\nabla}\cdot(\vec{q}_l C_l+\vec{q}_v C_v)T+\boldsymbol{\nabla}\cdot L_0\vec{q}_v-C_l S_h T, \tag{2.13}$$

where $C_l S_h T$ refers to the energy sink due to the root water uptake term.

2.3.3 Constitutive relations

2.3.3.1 Hydro-dynamical model relations

Liquid water content

The relation between liquid water content θ and capillary pressure head h is referred to as the *retention curve*. This curve differs with each different type of soil, and is regarded as a function of pore size distribution (Kuráž and Bloecher, 2017). The most famous and widely used model was the representation by Van Genuchten (1980) as:

$$\theta(h)=\begin{cases}\frac{\theta_s-\theta_r}{(1+(-\alpha_{vg}h)^{n_{vg}})^{m_{vg}}}+\theta_r, & \forall h\in(-\infty,0)\\ \theta_s, & \forall h\in\langle 0,+\infty),\end{cases} \tag{2.14}$$

where θ_s [-] is the saturated water content, θ_r [-] is the residual water content, α_{vg} [m^{-1}] is the inverse of the air entry value, and n_{vg}, m_{vg} [-] are the pore size distribution parameters.

Deriving the water retention curve function with respect to the pressure head h provides the so-called *retention soil water capacity* in the following formula:

$$C^l(h)=\begin{cases}\frac{\alpha_{vg}m_{vg}n_{vg}(-\alpha_{vg}h)^{n_{vg}-1}(\theta_s-\theta_r)}{(1+(-\alpha_{vg}h)^{n_{vg}})^{1+m_{vg}}}, & \forall h\in(-\infty,0)\\ 0, & \forall h\in\langle 0,+\infty).\end{cases} \tag{2.15}$$

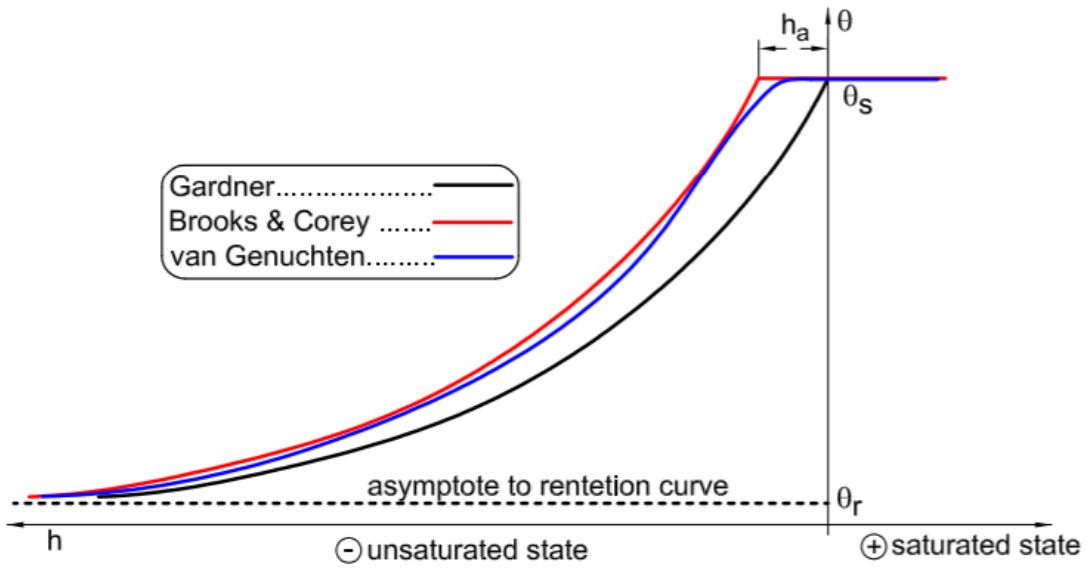

Figure 2.2: Water Retention Curve as in models by Gardner (1958), Brooks and Corey (1964) and Van Genuchten (1980), as depicted in Kuráž and Bloecher (2017).

Water vapor content

The equation describing water vapor content constitutes the reduction of the saturated vapor density by relative humidity and is given by:

$$\theta_v = (\theta_s - \theta_l) H_r \frac{\rho_{sv}}{\rho_l}, \tag{2.16}$$

where H_r [-] is the relative humidity, ρ_{sv} [kg.m^{-3}] is the saturated vapor density and ρ_l [kg.m^{-3}] is the liquid water density. Relative humidity as proposed by Philip and De Vries (1957) is:

$$H_r = \begin{cases} \exp\left(\frac{hMg}{RT}\right), & \text{if } h < 0 \\ 1, & \text{if } h \geq 0, \end{cases} \tag{2.17}$$

where h [m] is the capillary pressure head, $M = 0.018015$ [kg.mol^{-1}] is the molecular weight of water, g [m.s^{-2}] is the gravity acceleration, $R = 8.314$ [J.mol^{-1}.K^{-1}] is the universal gas constant , and T [K] refers to the temperature. The saturated vapor density is given as:

$$\rho_{sv} = 10^{-3} \frac{\exp\left(31.3716 - \frac{6014.79}{T} - 7.925 \times 10^{-3} T\right)}{T}, \tag{2.18}$$

where T [K] is the temperature in Kelvin. The liquid water density can be calculated from:

$$\rho_l = 1000 - 7.370 \times 10^{-3}(T - 3.98)^2 + 3.790 \times 10^{-5}(T - 3.98)^3. \tag{2.19}$$

The rest of the solution for equation (2.9) can be obtained by applying a product rule to derive the vapor water content with respect to h:

$$\frac{\mathrm{d}\theta_v}{\mathrm{d}h} = \frac{\mathrm{d}H_r}{\mathrm{d}h}\frac{\theta_s\rho_s}{\rho_l} - C^l(h)\frac{H_r\rho_{sv}}{\rho_l} - \frac{\mathrm{d}H_r}{\mathrm{d}h}\frac{\theta_l\rho_{sv}}{\rho_l}, \tag{2.20}$$

at this point we need to differentiate the relative humidity as follows:

$$\frac{\mathrm{d}H_r}{\mathrm{d}h} = \begin{cases} \frac{Mg}{RT}\exp\left(\frac{hMg}{RT}\right), & \text{if } h < 0 \\ 0, & \text{if } h \geq 0, \end{cases} \tag{2.21}$$

where the temperature T [K] is measured in Kelvin. Finally we need to differentiate water vapor content with respect to the temperature, which is also done by applying a product rule of three functions:

$$\frac{\mathrm{d}\theta_v}{\mathrm{d}T} = (\theta_s - \theta_l)\left(\frac{\mathrm{d}H_r}{\mathrm{d}T}\frac{\rho_{sv}}{\rho_l} + H_r\frac{\mathrm{d}\rho_{sv}}{\mathrm{d}T}\frac{1}{\rho_l} + H_r\rho_{sv}\frac{\mathrm{d}\frac{1}{\rho_l}}{\mathrm{d}T}\right), \tag{2.22}$$

then we derive relative humidity with respect to temperature as:

$$\frac{\mathrm{d}H_r}{\mathrm{d}T} = \begin{cases} -\frac{hMg}{RT^2}\exp\left(\frac{hMg}{RT}\right), & \text{if } h < 0 \\ 0, & \text{if } h \geq 0 \end{cases}. \tag{2.23}$$

The derivative of saturated vapor density with respect to T is given by:

$$\frac{\mathrm{d}\rho_{sv}}{\mathrm{d}T} = -\frac{(317T^2 + 40000T - 24059160)\exp\left(-\frac{317T}{4000} - \frac{60147}{100T} + \frac{78429}{250}\right)}{40000000T^3}, \tag{2.24}$$

and the derivative of $1/\rho_l$ is defined as:

$$\frac{\mathrm{d}(\rho_l^{-1})}{\mathrm{d}T} = -\frac{6250000000000(50T - 199)(56850T - 759626)}{(47375000T^3 - 9778157500T^2 + 75582816850T + 124985108356797)^2}. \tag{2.25}$$

Liquid water hydraulic conductivity

Deriving the water retention curve function provides the unsaturated hydraulic conductivity, which changes with different water content i.e., it changes with different pressure heads, since water content is dependant on pressure head (Kuráž and Bloecher, 2017). One of the most recognized formulas to describe the unsaturated hydraulic conductivity was introduced by Mualem (1976) which in the case of liquid water is stated as:

$$K_{lh}(h) = \begin{cases} K_s \frac{(1-(-\alpha_{vg}h)^{n_{vg}m_{vg}}(1+(-\alpha_{vg}h)^{n_{vg}})^{-m_{vg}})^2}{(1+(-\alpha_{vg}h)^{n_{vg}})^{\frac{m_{vg}}{2}}}, & \forall h \in (-\infty, 0) \\ K_s, & \forall h \in \langle 0, +\infty), \end{cases} \tag{2.26}$$

where K_s [m.s^{-1}] is the saturated hydraulic conductivity. The derivative of this term with respect to pressure head in this case is:

$$\frac{\mathrm{d}K_{lh}}{\mathrm{d}h} = \begin{cases} K_s \frac{1}{2}\alpha(-\alpha h)^{(-1+n)}(1+(-\alpha h)^n)^{(-1-m/2)}(1-(-\alpha h)^{(mn)} \\ (1+(-\alpha h)^n)^{(-m)})^2 mn + 2(1+(-\alpha h)^n)^{(-m/2)}(1-(-\alpha h)^{mn} \\ (1+(-\alpha h)^n)^{-m})(-\alpha(-\alpha h)^{(-1+n+mn)}(1+(-\alpha h)^n)^{(-1-m)}mn + \\ \alpha(-\alpha h)^{(-1+mn)}(1+(-\alpha h)^n)^{-m}mn), & \forall h \in (-\infty, 0) \\ 0, & \forall h \in \langle 0, +\infty). \end{cases} \tag{2.27}$$

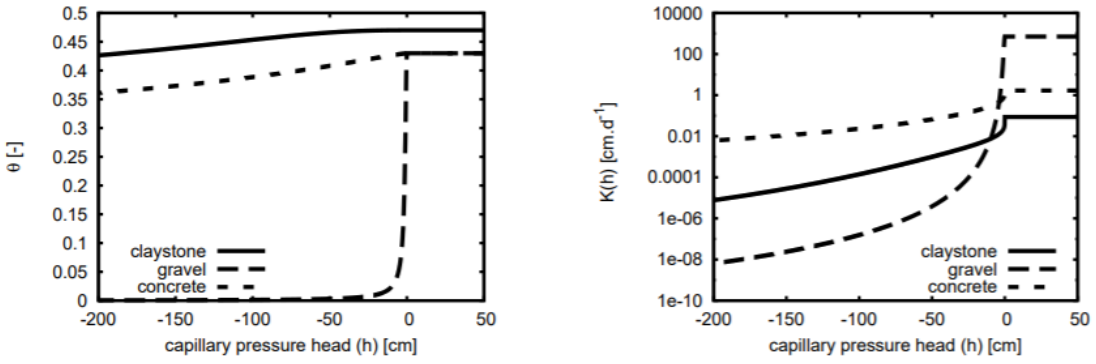

Figure 2.3: Constitutive relations of water retention curve (right) and unsaturated hydraulic conductivity (left) for different types of soil, where K_s is depicted in log scale (Kuráž and Bloecher, 2017).

Water vapor hydraulic conductivity

Nassar and Horton (1997) described the hydraulic conductivity of vapor as:

$$K_{vh} = \frac{D}{\rho_w}\rho_{sv}\frac{Mg}{RT}H_r, \tag{2.28}$$

where D [$m^2.s^{-1}$] is the vapor diffusivity in soil and is expressed as:

$$D = \tau(\theta_s - \theta_l)D_a, \tag{2.29}$$

where τ [-] is the tortuosity and D_a [$m^2.s^{-1}$] is the diffusivity of water vapor in air that depends on the temperature T [K]. Millington and Quirk (1961) described tortuosity as:

$$\tau = \frac{(\theta_s - \theta_l)^{7/3}}{\theta_s^2}, \tag{2.30}$$

and diffusivity of water vapor is defined as:

$$D_a = 2.120 \times 10^{-5}\left(\frac{T}{273.15}\right)^2, \tag{2.31}$$

where the temperature T is in [K].

Liquid hydro-thermal conductivity

Hydro-thermal conductivity is a cross term, and it is expressed as a response to the temperature gradient in the following form (K. Noborio et al., 1996):

$$K_{lT} = K_{lh}\left(hG_w\frac{1}{\gamma_0}\frac{\mathrm{d}\gamma}{\mathrm{d}T}\right), \tag{2.32}$$

where G_w [-] is the gain factor quantifying the temperature dependence of soil water retention curve and γ_0 [$g.s^{-2}$] is the surface retention at temperature = 25 °C. An average value of $G_w = 5.0$ as well as $\gamma_0 = 71.89$ [$g.s^{-2}$] were assigned (Kosuke Noborio et al., 1996; Nimmo and Miller, 1986). Finally, the derivative of surface tension with respect to temperature is given by:

$$\frac{\mathrm{d}\gamma}{\mathrm{d}T} = -0.1425 - 4.760 \times 10^{-4}T, \tag{2.33}$$

where the temperature T is measured in [°C].

Vapor hydro-thermal conductivity

Also a cross term, it is described in Sakai et al. (2011) as:

$$K_{vT} = \frac{D}{\rho_l}\eta H_r \frac{\mathrm{d}\rho_{sv}}{\mathrm{d}T}, \tag{2.34}$$

where η [-] is the enhancement factor and can be obtained from the formula defined by Jirka Simunek et al. (2005):

$$\eta = 9.5 + 3\frac{\theta_l}{\theta_s} - 8.5\exp\left(-\left((1+\frac{2.6}{\sqrt{f_c}})\frac{\theta_l}{\theta_s}\right)^4\right), \tag{2.35}$$

where f_c [-] is the mass fraction of clay in the soil which can never equal 0, and the exponential term can be neglected due to its very low values.

2.3.3.2 Thermodynamical model relations

Liquid volumetric specific heat capacity

A typical range for water temperature in soil is between 0-50 [°C]. Within these values, specific heat capacity of liquid is estimated to be $C_l^m = 4.16$ [kJ.Kg^{-1}.K^{-1}]. From that we can calculate volumetric specific heat capacity as:

$$C_l = C_l^m \rho_l T. \tag{2.36}$$

Solid volumetric specific heat capacity

Volumetric heat capacity of the soil C is typically presumed to be the sum of the volumetric heat capacities of all of the soil components. This can include organic matter, water, ice, air and even mineral grains (Kodešová et al., 2013). From the measured relationship between the volumetric heat capacity and the volumetric soil water content, and taking into account the correspondence between C and the fractions of the soil components, the solid volumetric heat capacity can be obtained as the values depicted in Table 1 of Kodešová et al. (2013).

Vapor volumetric specific heat capacity

For a normal water temperature range in soil (0-50 [°C]), specific heat capacity of vapor is estimated to be $C_v^m = 1.9$ [kJ.Kg^{-1}.K^{-1}]. From that we can calculate

volumetric specific heat capacity as:

$$C_v = C_v^m \rho_{sv} H_r. \tag{2.37}$$

Liquid volumetric latent heat of vaporizaton

The volumetric latent heat of vaporizaton for liquid water is expressed as:

$$L_0 = L\rho_l, \tag{2.38}$$

where L [J.kg^{-1}] is the latent heat of vaporization and is given as a function of temperature T [°C].

Thermal conductivity

Thermal conductivity is expressed as a function of water content (Simunek and Suarez, 1993):

$$\lambda(\theta) = \lambda_0(\theta) + \beta||\vec{q_l}||_2, \tag{2.39}$$

where β [m] is the thermal dispersivity. With the assumption of low flux values, β is negligible, and so $\lambda(\theta) = \lambda_0(\theta)$ which is described by Chung and Horton (1987) as:

$$\lambda(\theta) = b_1 + b_2\theta_l + b_3\sqrt{\theta_l}, \tag{2.40}$$

where b_1, b_2 and b_3 are regression empirical parameters given in Table 1 of Chung and Horton (1987).

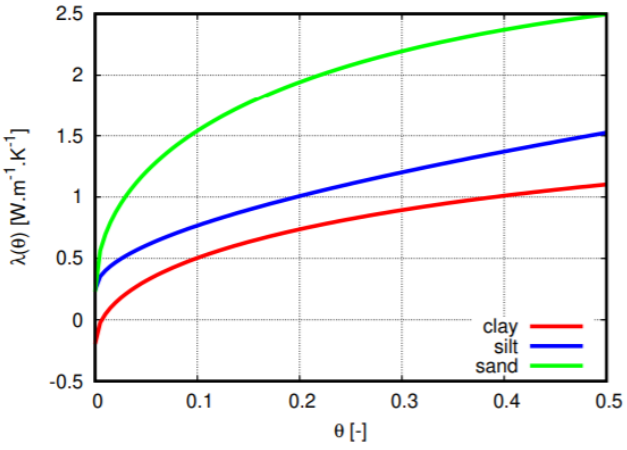

Figure 2.4: Thermal conductivity as a function of θ, as illustrated in Kuráž and Bloecher (2017). Note that for extremely dry clay λ may become negative.

Root water uptake

Feddes et al. (1978) developed a root water uptake model that defines the term as:

$$S = \alpha(h)\frac{S_{max}}{V_{roots}}, \tag{2.41}$$

where $\alpha(h)$ refers to a simplistic linear scale factor, V_{roots} [m^3] is the volume of root zone and S_{max} [$m^3.s^{-1}$] is the maximal plant transpiration. $\alpha(h)$ is known as the stress reduction function of matric potential. Its shape is defined by specific critical matric potentials h_0 to h_3 (Peters et al., 2017).

2.3.4 Initial Conditions

The state of the system at the beginning of computation is called the initial condition. In the case of coupled transport of water and heat, it is expressed as the value of the soil water content θ (or its pressure head) for the water flow, and described as:

$$h(x, t_0) = h_0(x), \qquad \forall x \in \Omega, \tag{2.42}$$

where Ω is the system's domain. While the initial condition for the heat flow is expressed as the value of temperature T:

$$T(x, t_0) = T_0(x), \qquad \forall x \in \Omega. \tag{2.43}$$

2.3.5 Boundary Conditions

Boundary conditions describe the specific conditions at the limits of our domain. There are three types of boundary conditions. A condition with a specific value of an independent variable, called *Dirichlet condition*, a known-flux (first order derivative of an independent variable) boundary condition (*Neumann Condition*), or a condition combining the previous two, which is termed *Robin condition*. Each condition requires its own approach. For example, to handle value-specified conditions, the equation of finite difference method takes the value at each specific time directly (Chung and Horton, 1987). The boundary conditions for the study of soil evaporation phenomenon can be divided into two groups; bottom boundary conditions (porous media or soil), and top boundary conditions (the atmosphere).

2.3.5.1 Porous medium boundary

A porous medium lower boundary in the problem of modelling soil evaporation can be set as a number of choices. These include a value-specified Dirichlet

condition, and a zero or nonzero flux Neumann's condition for both heat and water flow. Setting a zero Dirichlet's bottom condition for water flow would neglect the influence of a water table on the system. Likewise, assigning a zero temperature-gradient condition for heat flow assumes heat transfer by water convection only (Saito et al., 2006).
For this model's water flow, a free drainage lower boundary condition was chosen and expressed as:

$$\frac{\partial h}{\partial \vec{n}}(x,t) = 0, \qquad \forall x \in \Gamma_{bottom} \times (0,T\rangle, \tag{2.44}$$

while for heat flow, a zero-flux Neumann's condition was assigned initially, and described at depth z = 1 as:

$$\frac{\partial T(x,t)}{\partial \vec{n}} = 0, \qquad (z=1,t) \in \Gamma_{bottom} \times \langle 0, t_{end}). \tag{2.45}$$

This was later changed to Dirichlet boundary condition with constant value in the following form:

$$T(x,t) = 20, \qquad (z=1,t) \in \Gamma_{bottom} \times \langle 0, t_{end}). \tag{2.46}$$

2.3.5.2 Atmospheric interface boundary

While the soil surface heat flux constitutes the upper boundary condition for the heat flow, evaporation rate forms the top boundary for the water flow in this hydro-thermo-dynamic system. In order to obtain those conditions, the surface energy balance equation is needed (Sakai et al., 2011). The energy balance equation is a flux condition that is expressed in Chapter 2.1.3. A reformulation of equation (2.2) is given as:

$$R_n - H - LE - G = 0, \tag{2.47}$$

where R_n [W.m^{-2}] refers to the net radiation, H [W.m^{-2}] is the sensible heat flux density, LE [W.m^{-2}] is the latent heat flux density, and G [W.m^{-2}] is the surface heat flux density.

Radiation

When radiation reaches the atmosphere, a certain amount of it is reduced due to being reflected or absorbed by some elements (e.g clouds, gases). This amount is

also called *shortwave radiation* because of the short wavelengths energy emitted by the sun (Allen et al., 1998). The energy that the earth receives from solar radiation is reduced due to different processes (e.g radiation emission) via long wavelengths. Hence, this terrestrial radiation is also called *longwave radiation* (Allen et al., 1998). The difference between the longwave radiation that leaves the earth's surface (either to the atmosphere or lost into space) and the one received by the earth (which is exhibited as an increase in temperature) makes the total longwave radiation. Net longwave radiation always indicates a loss of energy since outgoing is bigger than incoming longwave radiation.

In Monteith and Unsworth (2013), net radiation is defined as the rate at which long or short wave radiation is received by a surface, and can be negative, positive, or zero according to losses or gains. The intensity of this radiation is dependant on the solar zenith angle, defined as the angle between the rays of the sun and its vertical or the normal to the atmosphere's surface. From Saito et al. (2006), net radiation can be given as:

$$R_n = R_{ns} + R_{nl}, \tag{2.48}$$

where R_{ns} [W.m^{-2}] is the net shortwave radiation and R_{nl} [W.m^{-2}] is the net longwave radiation. R_{ns} is given as:

$$R_{ns} = (1 - \alpha)R_{in}, \tag{2.49}$$

where R_{in} [W.m^{-2}] is the actual incoming global shortwave solar radiation, and α [-] is the albedo, a dimensionless unitless indication of the solar radiation reflection of a surface. Albedo measures how much of the total solar energy is reflected by the surface. It ranges from 0 signifying a black surface that absorbs all incoming radiation, to 1 which corresponds to a white body reflecting all radiation (Coakley, 2003). In Van Bavel and Hillel (1976), surface albedo is given as a simple linear expression dependant on surface water content:

$$\alpha = \begin{cases} 0.25, & \text{if } \theta_{top} < 0.1 \\ 0.10, & \text{if } \theta_{top} \geq 0.25 \\ 0.35 - \theta_{top}, & \text{if } \theta_{top} \in \langle 0.1, 0.25). \end{cases} \tag{2.50}$$

The net longwave radiation R_{nl} is defined as:

$$R_{nl} = \varepsilon_s R_{ld} \downarrow + R_{lu} \uparrow, \tag{2.51}$$

where $R_{ld}\downarrow$ refers to the longwave radiation incoming to the soil, and $R_{lu}\uparrow$ is the outgoing longwave radiation emitted from the soil to the atmosphere. ε_s [-] refers to the emissivity of the soil surface; the amount of longwave radiation reflected at the soil surface, and is defined by Van Bavel and Hillel (1976) as:

$$\varepsilon_s = \min(0.9 + 0.18\theta_{top}, 1.0). \tag{2.52}$$

The calculations and estimation procedure of incoming global shortwave solar radiation R_{in} will be treated further in Chapter 3.1.

Sensible heat

Van Bavel and Hillel (1976) proposed the following formula to calculate the sensible heat flux:

$$H = C_a \frac{(T_s - T_a)}{r_H}, \tag{2.53}$$

where C_a [J.m^{-3}.K^{-1}] is the volumetric heat capacity of air, T_s [K] is the soil surface temperature, T_a [K] is the air temperature, and r_H [$s.m^{-1}$] refers to the aerodynamic resistance to heat transfer and is defined as:

$$r_H = \frac{1}{kU^*}\left(\log\left(\frac{z_{ref} - d + z_H}{z_H}\right) + \Psi_H\right), \tag{2.54}$$

where U^* [m.s^{-1}] is the friction velocity, $k = 0.41$ [-] is the Karman constant, z_{ref} [m] is the reference height of the temperature measurement, $z_H = 1 \times 10^{-3}$ [m] is the surface roughness for the heat flux, d is the zero plane displacement, Ψ_H [-] is the atmospheric stability correction factor for the momentum flux, and is described by Camillo and Gurney (1986). the zero plane displacement is calculated as:

$$d = 2/3\ h, \tag{2.55}$$

where h [m] is the height of the plants (Allen et al., 1998). The friction velocity is given by

$$U^* = \frac{uk}{\log\left(\frac{z_{ref} - d + z_m}{z_m}\right) + \Psi_m}, \tag{2.56}$$

where u [m.s^{-1}]is the wind speed at the height z_{ref}, z_m [m] is the surface roughness for the momentum flux, and ψ_m [-] is the atmospheric stability correction factor for the momentum flux. The implementation of this numerical model assumes stable atmospheric conditions, and thus $\psi_h = \psi_m = 0$. Furthermore, the surface

roughness for the heat and momentum fluxes are described as:

$$z_m = 0.123\ h, \tag{2.57}$$

$$z_H = 0.1\ h. \tag{2.58}$$

Latent heat

The latent heat flux density LE is made up of the latent heat L [J.kg^{-1}] and the evaporation rate E [kg.m^{-2}.s^{-1}]. Saito et al. (2006) defines the equation for the latent heat as:

$$L = 2.501 \times 10^6 - 2369.2T, \tag{2.59}$$

where T [°C] represents the air temperature. In Van Bavel and Hillel (1976), authors indicate the influence of factors such as surface wetness, atmospheric conditions, and the transport of moisture in the soil from the equation suggested to calculate the rate of evaporation:

$$E = \frac{\rho_{vs} - \rho_{va}}{r_H + r_s}, \tag{2.60}$$

where ρ_{vs} [kg.m^{-3}] is the density of water vapor at the soil surface, ρ_{va} [kg.m^{-3}] is the density of the atmospheric vapor, and r_s [s.m^{-1}] refers to the resistance of soil surface to water vapor flow, expressed as:

$$r_s = -805 + 4140(\theta_s - \theta_{top}). \tag{2.61}$$

This resistance is often neglected in evaporation models that only consider the aerodynamic resistance. However, this method might overestimate the rate of evaporation when the soil is dry. This is due to the assumption of equilibrium between the liquid phases and vapor phases of water in the soil that is made in the equation calculating the relative humidity H_r. The physical reality is that in dry soil surfaces, water vapor is transferred dynamically from larger pores to the atmosphere, disturbing the equilibrium between vapor density in pores and the average water content at a certain depth.

Chapter 3

Methodology

3.1 Estimation of Solar Radiation

Since no direct measurement of solar shortwave radiation was provided, this variable that composes a term in the solution to the surface energy balance needed to be estimated. To calculate actual incoming shortwave radiation, relative sunshine duration must be taken into account. Referring to the Angstrom formula (Ångström, 1929), R_{in} can be expressed as:

$$R_{in} = (a_s + b_s)R_s, \tag{3.1}$$

where R_s [W.m^{-2}] is the shortwave radiation received at the surface of the earth and a_s, b_s are regression constants representing the fraction of extraterrestrial radiation reaching the earth. Shortwave radiation that the earth's surface receives is dependant on the time and location of the surface. This is because the intensity of radiation is influenced by the sun's position. The effect of different latitudes and seasons can be factored in by including the solar elevation angle in the computation of R_s as follows:

$$R_s = \max\Big(\sin(e)R_a, 0\Big), \tag{3.2}$$

where R_a [W.m^{-2}] is the potential extraterrestrial radiation, and e [rad] is the solar elevation angle. Monteith and Unsworth (2013) define the zenith angle of the sun as the angle between the sun's direction and its vertical, and is complimentary to the angle e. The two angles are what cause the diurnal changes of radiation

between day and night. Thus, the solar elevation angle is formulated as:

$$\sin(e) = \sin(\varphi)\sin(\delta) + \cos(\varphi)\cos(\delta)\cos\left(\frac{2\pi(t-12)}{24}\right), \tag{3.3}$$

where φ [rad] is the latitude, δ [rad] is the solar declination, and t is the local time within a day. Finally, potential extraterrestrial radiation is the radiation that is received at the top of the atmosphere on a horizontal surface. This is given by:

$$R_a = \frac{G_{sc} d_r}{\pi}(\omega_s \sin(\varphi)\sin(\delta) + \cos(\varphi)\cos(\delta)\sin(\omega_s)), \tag{3.4}$$

where $G_{sc} = 1360$ [W.m^{-2}] is the solar constant, d_r is the inverse relative distance between Earth and the sun, and ω_s [rad] is the sunset hour angle. Equations to compute the solar declination δ and the sunset hour angle ω_s are expressed in Allen et al. (1998) as follows:

$$\delta = 0.409 \sin\left(\frac{2\pi}{365}J - 1.39\right), \tag{3.5}$$

$$\omega_s = \arccos(-\tan(\varphi)\tan(\delta)), \tag{3.6}$$

and the inverse relative sun-earth distance equation is also given by Allen et al. (1998) as:

$$d_r = 1 + 0.033 \cos\left(\frac{2\pi}{365}J\right), \tag{3.7}$$

where J is the number of the day in the year. This is estimated using the formula:

$$J = (275M/9 - 30 + D) - 2, \tag{3.8}$$

where M is the month and D is the day and then:

$$J = \begin{cases} J+2, & \text{if } M < 3 \\ J+1, & \text{if } M > 2 \text{ and Y is a leap year.} \end{cases} \tag{3.9}$$

3.2 Tools for Input Automation

3.2.1 Observations automated tool

For the purpose of model evaluation, in-situ measurements of some key-features of the evaporation process are required for observations comparison (e.g pressure head and soil temperature). These parameters can usually be taken from soil

sensors that record readings with a certain frequency. In order to obtain the measurements in a computation-ready form, I created a data-retrieval tool that connects to the API (Application Programming Interface) of the soil sensors (for this case study these were provided by *Lesprojekt-Služby* Ltd, 2021 company), via a communication protocol. I used Python programming language to write a code that generates a file containing observation records in an easy-to-access format. As Figure 3.1 illustrates, the program takes an input of a source link to the platform on which the sensors readings are uploaded in a JSON format. JSON is a semi-structured data format that stores data objects in a *Key:Value* mode. This raw data contains various sensor readings with the sensor ID, time and value of the measurement. The measured phenomenon name and unit of the parameter are stored on another platform with its own API, which I use to assign physical meaning to each sensor ID. The program I created has two modes for requested time-frame: either daily access-and-capture (i.e., the previous day's measurements), or historical access according to the user's chosen start and end dates. Next, the program retrieves the JSON file from the provided API and starts to parse through. This includes: a. Initial conversion to a more structured form by separating the content to columns where the *'Key'* attribute translates into headers and each *'Value'* attribute is stored consecutively in the column's cells, and B. Converting time stamps into computer-readable date-time format. After that the cleaning and verifying procedure starts. Because of the nature of JSON files, standard syntax analysis may result in a faulty outcome. For example, some of the measurement records may be missing, either due to sensor failure or electricity shortage. That also leads to incorrect assignment of a certain value to a sensor ID while parsing. Therefore, I built an inspect-and-flag procedure in R language to identify missing or otherwise falsely-marked attributes. This is composed of plotting the observations to detect any inexplicable oscillations, and pulling the maximum and minimum value of each parameter to ascertain the validity of its range.

The following step consists of computing the pressure head h value from the measured soil water potential at each measurement step using the following equation:

$$h = \frac{\psi}{\rho g}, \tag{3.10}$$

where ψ [Pa] is the soil water potential which can be converted to [kg.m^{-1}.s^{-2}], ρ [kg.m^{-3}] is water density, and g [m.s^{-2}] is the gravity acceleration. Finally, a structured CSV form is constructed and a CSV file is generated as the output of the code, containing the time step in seconds, soil water potential, pressure head, and soil temperature values at every step at the depths of two soil sensors, along

with the time of measurement.

3.2.2 Input generation tool

The solution to the surface energy balance equation requires the knowledge of a number of meteorological parameters such as incoming shortwave radiation, relative humidity, wind speed, and air temperature. Those variables are used as an input to the evaporation module in the form of the *ebalance.in* file. In order to generate this input file, I developed a Python program that constructs a table containing those parameters using information from a weather server. The input to this program is a link to the weather forecasting service (for this case study this was the national weather service of Argentina SMN, 2020). First, the code requests the specific file of daily weather data, which comes in a zipped form. Second, the file is downloaded and extracted, and this record is saved for later analysis. Following this, the file is parsed through to identify the set of data for the specific required location. After retrieving the specified information, it is subjected to cleaning in order to prepare it for further computations (e.g., removing undesirable spaces and skip-line hidden commands). The Python script then generates a base file consisting of this prepared data. Since measurement units can vary between different countries according to many systems, the next step I wrote in the program was unit conversion. Afterwards, and due to the lack of any radiation measurements from the weather server, calculations of the incoming solar (shortwave) radiation was also included in the tasks performed by this program. This was done in three main steps:

1. Calculation of the extraterrestrial radiation R_a reaching the top of the atmosphere, which factors in the angle between the sun's rays direction and the normal to the atmosphere's surface.

2. Calculation of the solar shortwave radiation R_s, reaching the horizontal earth's plane. This is derived from R_a, taking into account its variable intensity according to the time and location (due to the changing position of the sun).

3. Calculation of the actual incoming shortwave radiation R_{in}, which is taken from R_s after accounting for the cloudiness (i.e., the relative sunshine duration) of the day.

The actual incoming shortwave radiation R_{in} is the parameter ultimately used in computing the solution for the surface energy balance equation (explained more in Chapter 2.3). The full procedure of estimating the incoming solar radiation,

including all the relevant equations, is detailed in Chapter 3.1. The last step the code executes is constructing the *ebalance.in* file, containing the required meteorological information to be used for the evaporation model.
Since most of the weather services record daily measurements, I added an option of merging several daily records into one that can be used to create the needed data over a longer period of time. This option can be especially crucial when access to server archive is unavailable, due to the length of the time frame required to model the process of evaporation. Figure 3.2 shows the flowchart of the code execution.

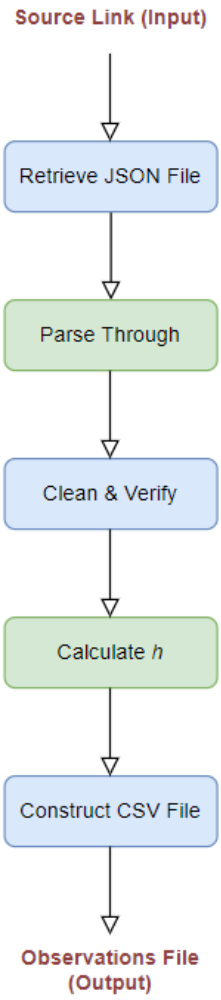

Figure 3.1: Flowchart of generating the observations file in the CSV format.

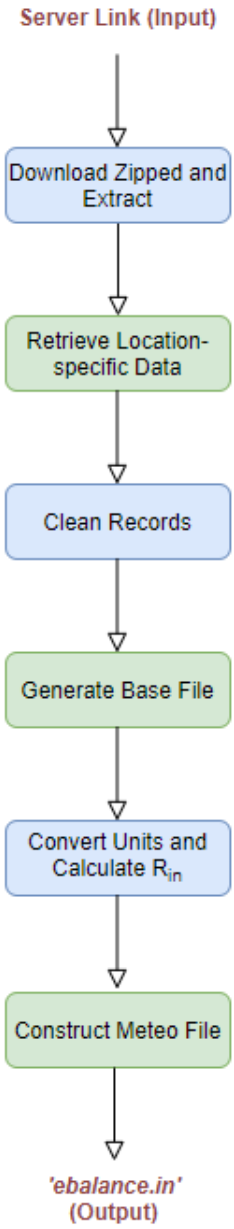

Figure 3.2: Flowchart of constructing the *ebalance.in* file using Python script.

3.3 Case Study

3.3.1 Site description

In order to determine the model's efficiency, data from two sensors installed in a commercial vineyard in San Juan, Argentina (31.5351°S, 68.5386°W) was collected. The vineyard is irrigated via 100 m-distanced pipes using water brought to it by trucks and is often over-saturated. The sensors are installed at the depths of 0.35 and 0.8 m below surface (average slope of the surface is 0.5%). Temperature

ranges between 1°C and 16 °C in the winter, and 19°C and 35°C in the summer. Year-round average sunlight is 76% of possible sunshine, and an average monthly precipitation ranges from 1.6 to 18.9 mm. Soil profile was set to be 1 m deep, and is illustrated in Table 3.1 with the root zone mostly covering depths between 0.1 and 0.5 m. Figure 3.3 explains the composition of different soil textures.

Table 3.1: Soil profile formation in the 1 m domain where the layers start with 0 m at the surface and progress downwards.

Soil Composition	Depth	Layer
Sand	0.8 - 1 m	1
Heavy clay	0.7 - 0.8 m	2
Silty clay loam, no roots	0.5 - 0.7 m	3
Silty clay loam, roots present	0.2 - 0.5 m	4
Silty clay loam with 1-2% organic matter, roots present	0.1 - 0.2 m	5
Silty clay loam with 1-2% organic matter, no roots	0 - 0.1 m	6

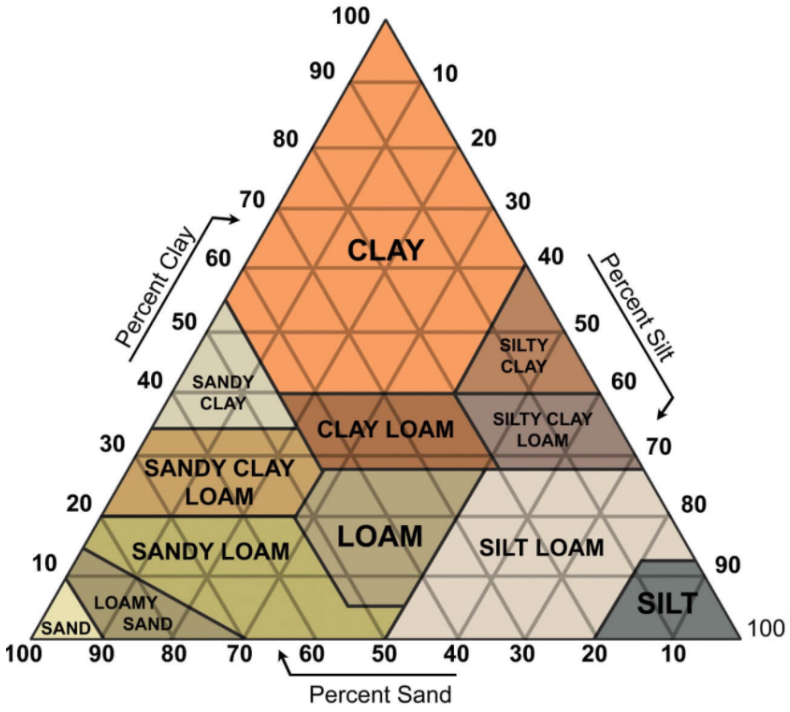

Figure 3.3: Soil texture diagram: different fractions of sand, silt and clay particles that compose different types of soil as illustrated in Shahid et al. (2018).

3.3.2 First simulation

A calibration period was chosen to start immediately before evaporation starts (noted by decreasing of the soil water potential), and end right before an irrigation event. This is due to the influence irrigation has on the boundary and initial conditions of the system. I was able to detect this information from the observation table generated using the automated measurement tool, and the simulation setup was assigned to be the period between 26 Nov. 2020, and 10 Dec. 2020. The domain was divided into six layers, noted down in Table 3.1, depending on soil type and root zone density. Figure 3.4 illustrates the diagram of the layers with the location of the soil sensors used for obtaining the domain's initial conditions.

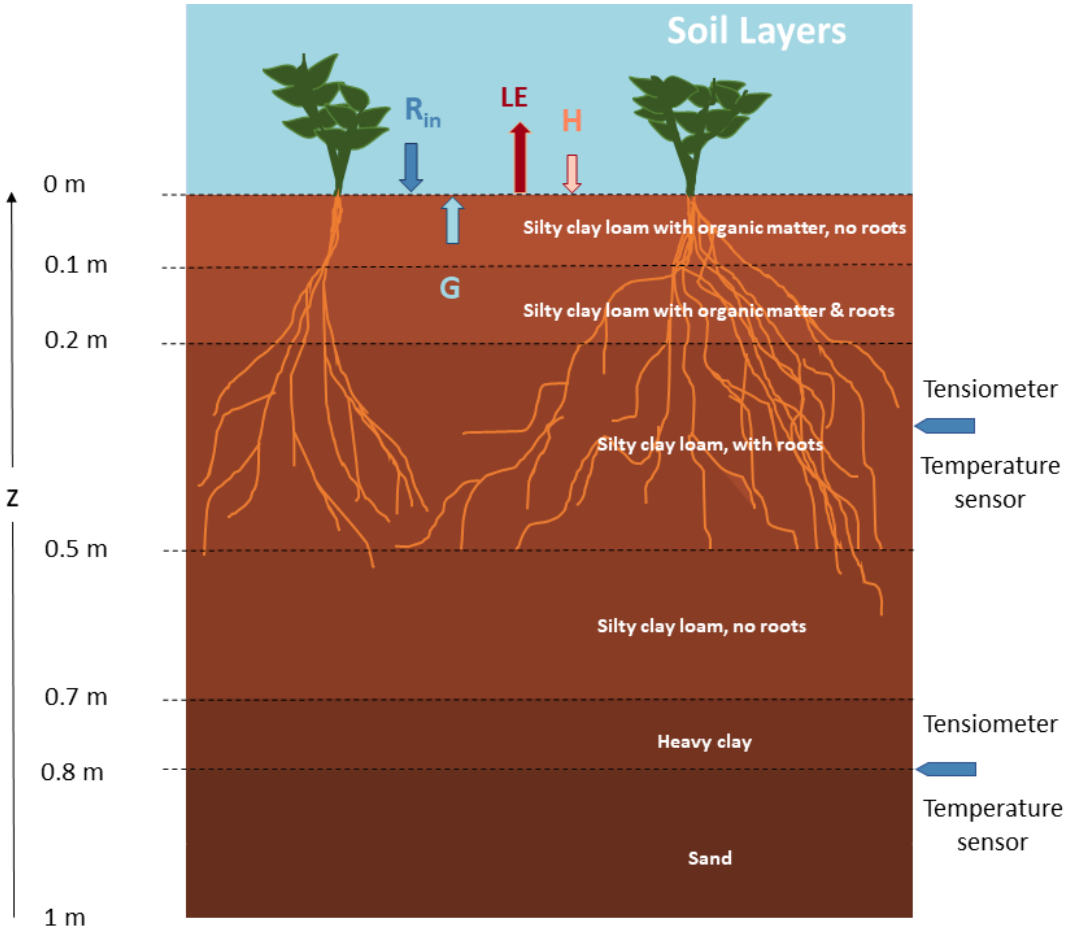

Figure 3.4: Soil layers scheme at the case study site. Tensiometer and soil temperature sensors are installed at the depths of 0.35 and 0.8 m.

3.3.2.1 Parameterization of water transport

To setup the water flow model, parameters for the water retention curve were assigned using *Rosetta* (Schaap et al., 2001). Rosetta is a computer program developed by M.G. Schaap to estimate soil hydraulic parameters such as water retention, saturated, and unsaturated conductivity. Table 3.2 shows the van Genuchten parameters as well as the saturated hydraulic conductivity values determined at each layer. Pressure head was chosen to be the initial boundary condition, mimicking h values measured at the sight by soil sensors and mathematically formulated as:

$$h(x,0) = -1, \qquad \forall x \in \Omega, \tag{3.11}$$

where $\Omega \in (0,1)$ m is the system's domain. The top boundary of the domain is assigned as an atmospheric condition (for the unknown pressure head this equals the evaporation rate), calculated based on meteorological data that is fed into equations solving the surface energy balance which are explained in Chapter 2.3.5.2. This Neumann-type condition is expressed as:

$$K(h)\left(\frac{\partial h(x,t)}{\partial \vec{n}} + n_3(x)\right) = E_{surf}(t), \quad (z=0,t) \in \Gamma_{top} \times \langle 0, t_{end}). \tag{3.12}$$

Free drainage was set as the bottom boundary condition,and described as follows:

$$\frac{\partial h}{\partial \vec{n}}(x,t) = 0, \quad \forall x \in \Gamma_{bottom} \times (0, t_{end}\rangle. \tag{3.13}$$

Table 3.2: Van Genuchten parameters assigned in the 1^{st} simulation as part of the water transport model description.

Layer	Parameter	Value	Unit
1	Inverse of air entry value α	3.5	[m^{-1}]
	Shape parameter n	3.2	[-]
	Residual water content θ_r	0.053	[-]
	Saturated water content θ_s	0.375	[-]
	Saturated hydraulic conductivity K_s	7.4e-5	[$m.s^{-1}$]
2	Inverse of air entry value α	1.5	[m^{-1}]
	Shape parameter n	1.25	[-]
	Residual water content θ_r	0.098	[-]
	Saturated water content θ_s	0.459	[-]
	Saturated hydraulic conductivity K_s	1.71e-6	[$m.s^{-1}$]
3 - 6	Inverse of air entry value α	0.84	[m^{-1}]
	Shape parameter n	1.52	[-]
	Residual water content θ_r	0.090	[-]
	Saturated water content θ_s	0.482	[-]
	Saturated hydraulic conductivity K_s	1.29e-6	[$m.s^{-1}$]

3.3.2.2 Parameterization of heat transport

The thermal conductivity equation (2.40), which drives the heat flux independently of water, includes three regression parameters. Those are empirical parameters, the values of which were chosen according to Chung and Horton (1987), under the assumption that organic matter in the surface layer is negligible, and that silt is the dominant particle in the silty clay loam layers. Initial boundary was set as a temperature value taken from in-situ measurements and can be defined as:

$$T(x, 0) = 21.8, \qquad \forall x \in \Omega_{top}, \tag{3.14}$$

where Ω_{top} is the (0,0.5) m domain of the top 3 layers, and as:

$$T(x,0) = 20.3, \qquad \forall x \in \Omega_{bottom}, \tag{3.15}$$

where Ω_{bottom} is the domain of (0.5,1) m i.e., the bottom 3 layers. In terms of boundary conditions, the top boundary was similar to water transport (assigned as the soil surface heat flux and evaluated as part of the surface energy balance computation), described as:

$$\frac{\partial T(x,t)}{\partial \vec{n}} = G_{surf}, \quad (z = 0, t) \in \Gamma_{top} \times \langle 0, t_{end}), \tag{3.16}$$

while zero-gradient Neumann boundary was assigned at the bottom for heat flow following the mathematical formula:

$$\frac{\partial T(x,t)}{\partial \vec{n}} = 0, \qquad \forall x \in \Gamma_{bottom} \times (0, t_{end}\rangle. \tag{3.17}$$

For calculations of the volumetric heat capacity of soil, knowledge of soil's specific heat capacity and density are needed. According to Kodešová et al. (2013), soil minerals' specific heat capacity = 730 [J.kg^{-1}.K^{-1}], and that of organic matter = 1900 [J.kg^{-1}.K^{-1}],. Since density of the soil is not known, it was assumed to be that of a sandstone made of quartz. As for the liquid, the specific heat of water is given. Table 3.3 contains the chosen parameters for this model.

Table 3.3: Heat model parameters assigned in the 1^{st} simulation. Sand, clay, and silt are assumed for layers 1, 2, and 3-6 respectively.

Layer	Parameter	Value	Unit
1	Empirical parameter b_1	0.228	[W.m^{-1}.K^{-1}]
	Empirical parameter b_2	-2.406	[W.m^{-1}.K^{-1}]
	Empirical parameter b_3	4.909	[W.m^{-1}.K^{-1}]
	Specific heat capacity of soil C_s	2.545e6	[J.m^{-3}.K^{-1}]
2	Empirical parameter b_1	-0.197	[W.m^{-1}.K^{-1}]
	Empirical parameter b_2	-0.967	[W.m^{-1}.K^{-1}]
	Empirical parameter b_3	2.521	[W.m^{-1}.K^{-1}]
	Specific heat capacity of soil C_s	2.545e6	[J.m^{-3}.K^{-1}]
3 - 6	Empirical parameter b_1	0.243	[W.m^{-1}.K^{-1}]
	Empirical parameter b_2	0.393	[W.m^{-1}.K^{-1}]
	Empirical parameter b_3	1.534	[W.m^{-1}.K^{-1}]
	Specific heat capacity of soil C_s	2.545e6	[J.m^{-3}.K^{-1}]

3.3.3 Second simulation

After the initial calibration, a second parameter-trial was conducted. I opted to increase the values of K_s, and decrease the van Genuchten parameters as well as the conductivity of root water uptake evident in maximum plant transpiration. Since the soil is made up of silty clay loam, initial assumption of silt dominance in the layers above sand was changed to correspond with a clay-type soil reflected in the values of thermal conductivity parameter b_1, b_2, and b_3. To account for the different soil layer types, the value of soil heat capacity was also decreased, while taking into account the presence of roots as organic material in the soil. Finally, the lower boundary for the heat flow was changed to Dirichlet with a constant value to better reflect the physical state of the system, and was mathematically expressed as:

$$T(x,t) = 20 \qquad (z = 1, t) \in \Gamma_{bottom} \times \langle 0, t_{end}). \tag{3.18}$$

Tables 3.4 and 3.5 includes the original and the optimized values of the

changed parameters over the same period of simulation.

Table 3.4: Optimized van Genuchten parameters assigned in the 2^{nd} simulation as part of the water transport model description.

Layer	Parameter	Initial Value	Optimized Value	Unit
1	Inverse of air entry value α	3.5	2.5	[m^{-1}]
	Shape parameter n	3.2	2.2	[-]
	Shape parameter m	0.69	0.6	[-]
	Sat. hydraulic conductivity K_s	7.4e-5	2.4e-4	[$m.s^{-1}$]
2	Inverse of air entry value α	1.5	0.1	[m^{-1}]
	Sat. water content θ_s	0.459	0.55	[-]
	Sat. hydraulic conductivity K_s	1.71e-6	12.90e-7	[$m.s^{-1}$]
5 - 6	Inverse of air entry value α	0.84	0.5	[m^{-1}]
	Shape parameter n	1.52	1.3	[-]
	Shape parameter m	0.34	0.23	[-]
	Sat. water content θ_s	0.482	0.54	[-]

Table 3.5: Optimized heat model parameters assigned in the 2^{nd} simulation. Sand is assumed for the first layer and clay for layers 2-6.

Layer	Parameter	Initial Value	Optimized Value	Unit
1 - 4	Specific heat capacity of soil C_s	2.545e6	1.6e6	[$J.m^{-3}.K^{-1}$]
3 - 6	Empirical parameter b_1	0.243	-0.197	[$W.m^{-1}.K^{-1}$]
	Empirical parameter b_2	0.393	-0.967	[$W.m^{-1}.K^{-1}$]
	Empirical parameter b_3	1.534	2.521	[$W.m^{-1}.K^{-1}$]
5 - 6	Specific heat capacity of soil C_s	2.545e6	2.0e6	[$J.m^{-3}.K^{-1}$]

3.3.4 Hydraulic conductivity senstivity analysis

For the purpose of optimizing the model's performance, sensitivity tests was performed to determine the influence of saturated hydraulic conductivity K_s on estimating the evaporation rate. This was done by altering the value of K_s within a certain range, and investigating the effects this had on the simulated pressure head and soil temperature. The original pressure head prediction and the prediction with modified K_s were compared using R programming language. Hydraulic conductivity was varied in both a positive and a negative direction to determine the impact of an up-to-2 orders of magnitude increase/decrease K_s. However, increasing the value of hydraulic conductivities from the initial magnitude detailed in Table 3.2 lead to model convergence issues independent of the estimation of the pressure head. The modified values are summarized in Table 3.6.

Table 3.6: Sensitivity tests conducted on saturated hydraulic conductivity to investigate the effect of K_s on the result's of the model.

Test	**Parameter**	**Layer**	**New value**	**Unit**
First	Saturated Hydraulic conductivity K_s	1	7.4e-6	[m.s^{-1}]
		2	1.71e-7	[m.s^{-1}]
		3 - 6	1.29e-7	[m.s^{-1}]
Second	Saturated Hydraulic conductivity K_s	1	7.4e-7	[m.s^{-1}]
		2	1.71e-8	[m.s^{-1}]
		3 - 6	1.29e-8	[m.s^{-1}]

Chapter 4

Results

4.1 Model Calibration

4.1.1 Pressure Head

During the investigation of this study results, a plot analysis of observations versus simulations was carried out. Figure 4.1 shows the simulated pressure head values at depths (a) 0.35 m and (b) 0.8 m, resulting from the first calibration scenario explained in Chapter 3.3.2. While the setup mimicked the start and end values of h at the depth of 0.35 m well, the rest of the experiment duration saw an underestimation of the evaporation rate. As for the simulation of pressure head at 0.8 m, the model both underestimated and overestimated h for most of the simulation period. To rectify the overestimation of evaporation rate, a number of options were considered. One being to increase the value of K_s, which had a big influence on the initial stage of the simulation. Another way was to change the van Genuchten parameters α and n that control the shape of the water retention curve, which was the choice employed in the second scenario of the simulation. The final configuration was a combination of those two methods, as Tables 3.4 and 3.5 detail. With this setup, model-predicted values approximated observations well. The accuracy of the simulated h at depth 0.35 m is evident in Figure 4.2, and while the values are not as precise at the other observation point (0.8 m), the results still improve from that of the first calibration run.

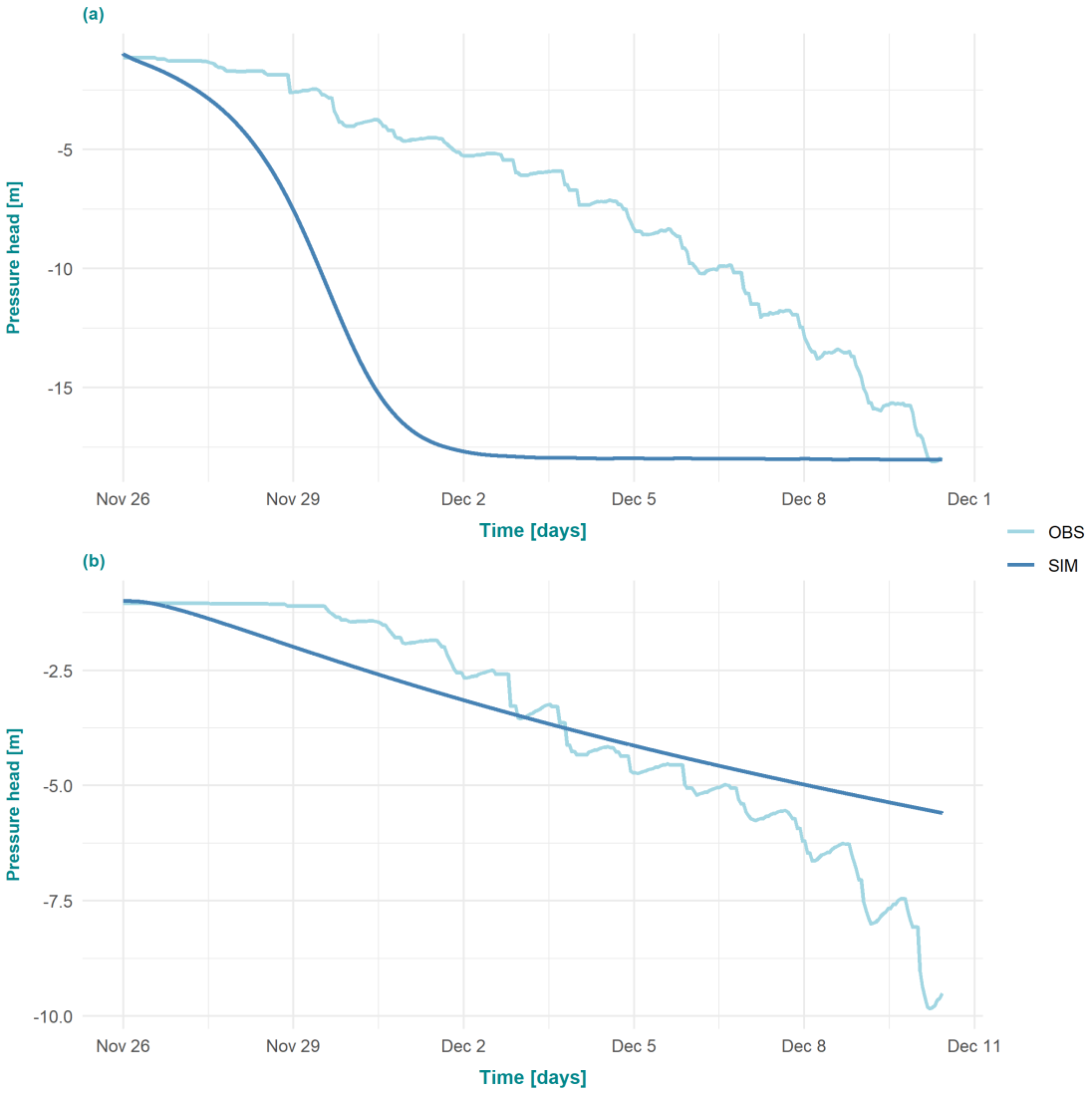

Figure 4.1: Simulated versus observed pressure head at depths (a) 0.35 m and (b) 0.8 m during the first calibration scenario (26 Nov. 2020 - 10 Dec. 2020).

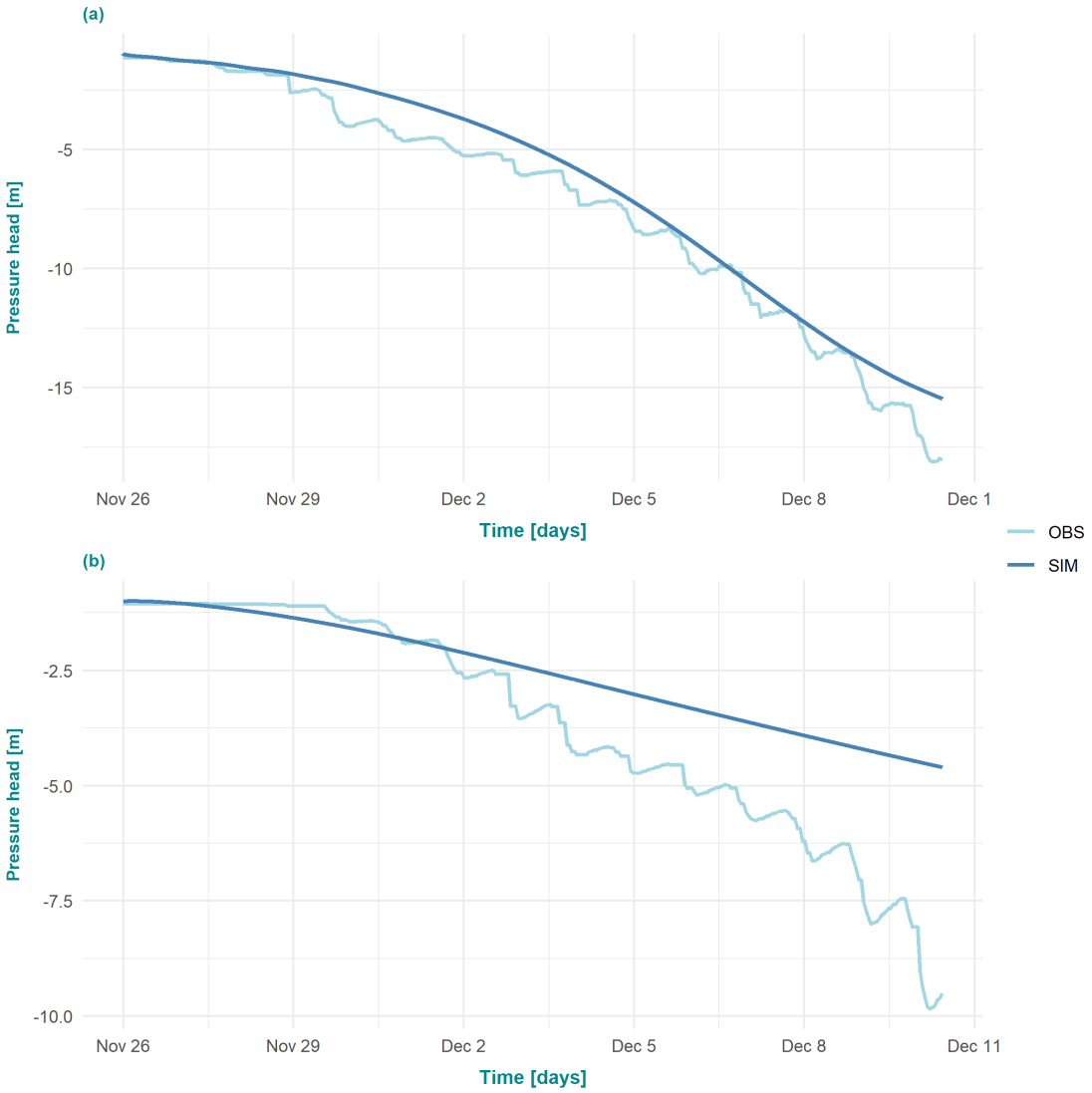

Figure 4.2: Simulated versus observed pressure head at depths (a) 0.35 m and (b) 0.8 m during the second calibration scenario (26 Nov. 2020 - 10 Dec. 2020).

4.1.2 Temperature

In terms of soil temperature, the first simulation scenario can be seen in Figure 4.3 which plots model values against measured values at the two soil-sensor depths. The prediction of the first 5 days for T at the depth of 0.35 m compared well with the measured values. However, there was a clear rise above observations in the rest of the period as well as the entire simulation at the second sensor's depth (0.8 m). Evidently, overestimating evaporation had a vivid influence not only on the simulated h, but also on the soil temperature values. This was rectified in the second simulation run where model-generated soil temperature at the two depths followed real-life observations with better precision, as illustrated by Figure 4.4.

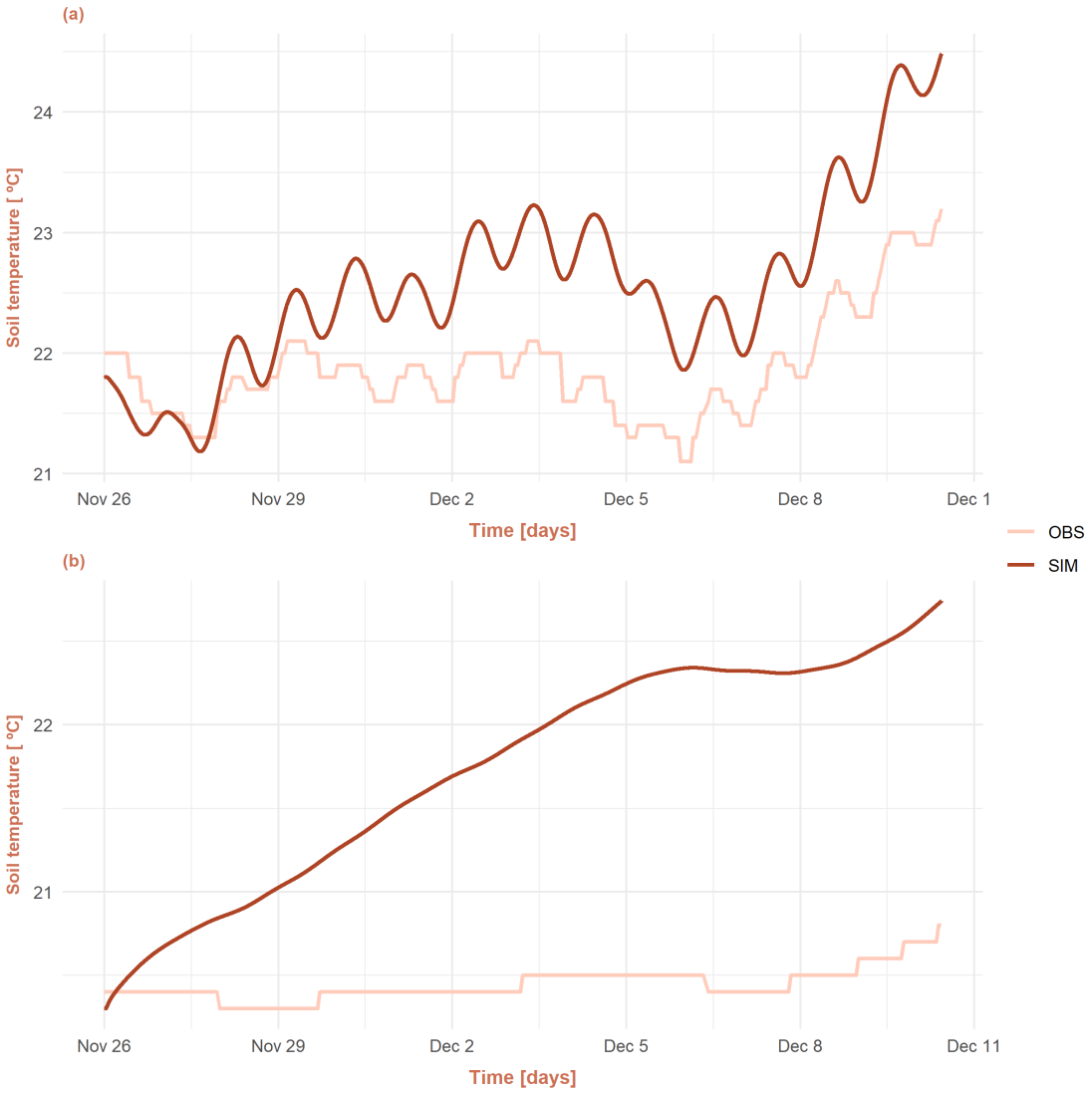

Figure 4.3: Simulated versus observed soil temperature at depths (a) 0.35 m and (b) 0.8 m during the first calibration scenario (26 Nov. 2020 - 10 Dec. 2020).

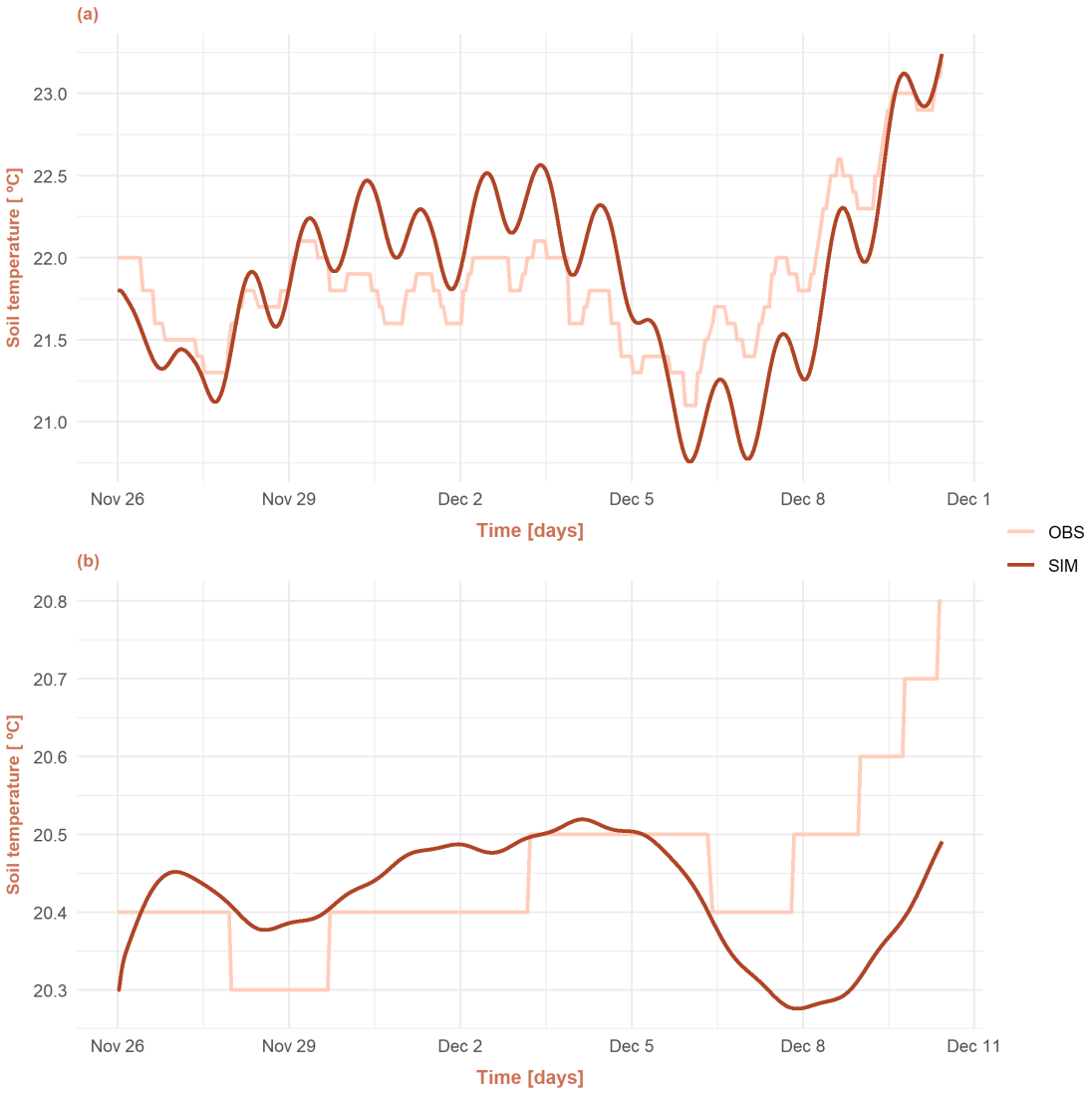

Figure 4.4: Simulated versus observed soil temperature at depths (a) 0.35 m and (b) 0.8 m during the second calibration scenario (26 Nov. 2020 - 10 Dec. 2020).

4.1.3 Solar Radiation

Solar radiation is one of the most important terms in creating the solution to the surface energy balance equation. The equations incorporated to obtain the value of incoming shortwave solar radiation were explained in Chapter 3.1. Net radiation values that are computed as a part of the model's output are reflected in the surface energy balance parameters' estimation and shown by Figure 4.5. The plot illustrates the relation between different heat fluxes and projects the diurnal changes caused by alternations between day and night.

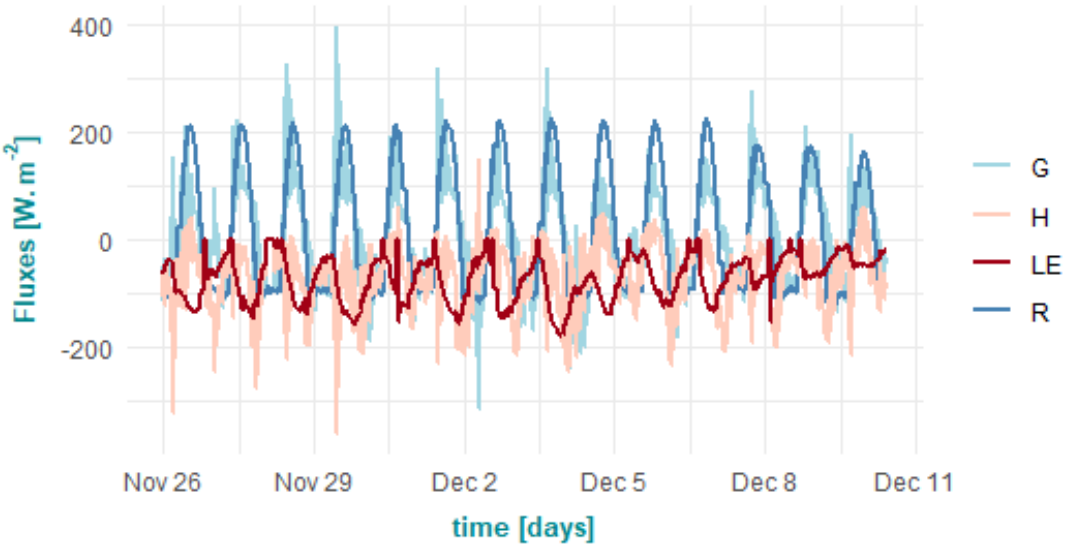

Figure 4.5: Solution of the surface energy balance equation, where the surface heat flux G is calculated by subtracting the sensible heat flux H and the latent heat flux LE from the net radiation R (26 Nov. 2020 - 10 Dec. 2020).

4.1.4 Evaporation rates

Evaporation rates were characterized by solving the surface energy balance equation (see Equation 2.47) and thus acquiring the upper boundary flux condition (Neumann condition) for the unknown pressure head in the water transport model. Figure 4.6 depicts the calculated evaporation rate at the vineyard study site during the model's calibration period.

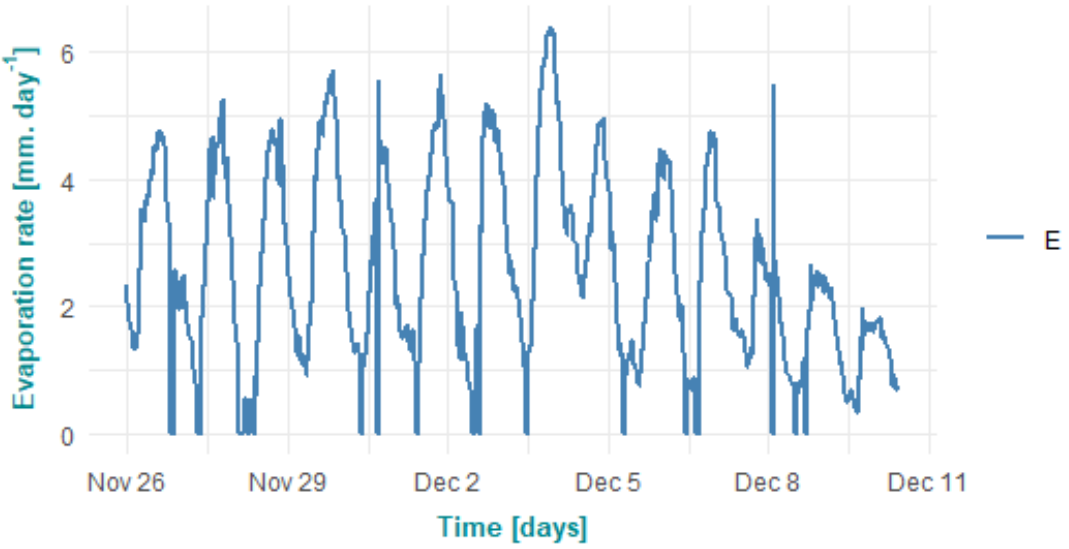

Figure 4.6: Evaporation rate estimation during the calibration scenario (26 Nov. 2020 - 10 Dec. 2020)

4.2 Model Verification

In order to verify the developed model, another evaporation scenario was chosen for simulation. As with the calibration setup, the start and end time of this simulation period was selected between irrigation events, to avoid any interference with the conditions of the system. Soil temperature and pressure head were simulated numerically from 16 Feb. 2021 until 22 Feb. 2021.

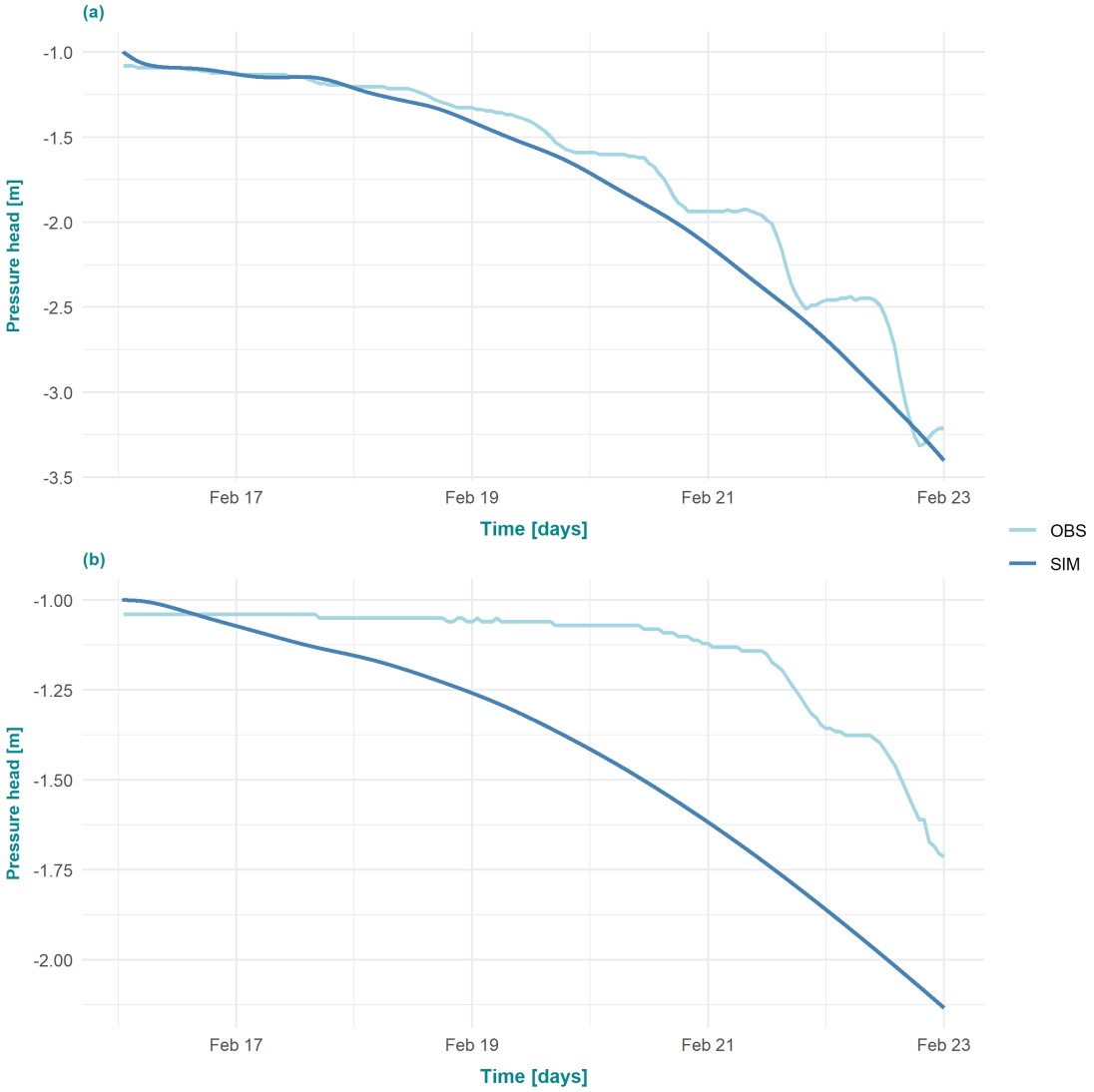

Figure 4.7: Simulated versus observed pressure head at depths (a) 0.35 m and (b) 0.8 m during the validation scenario (16 Feb. 2021 - 22 Feb. 2021).

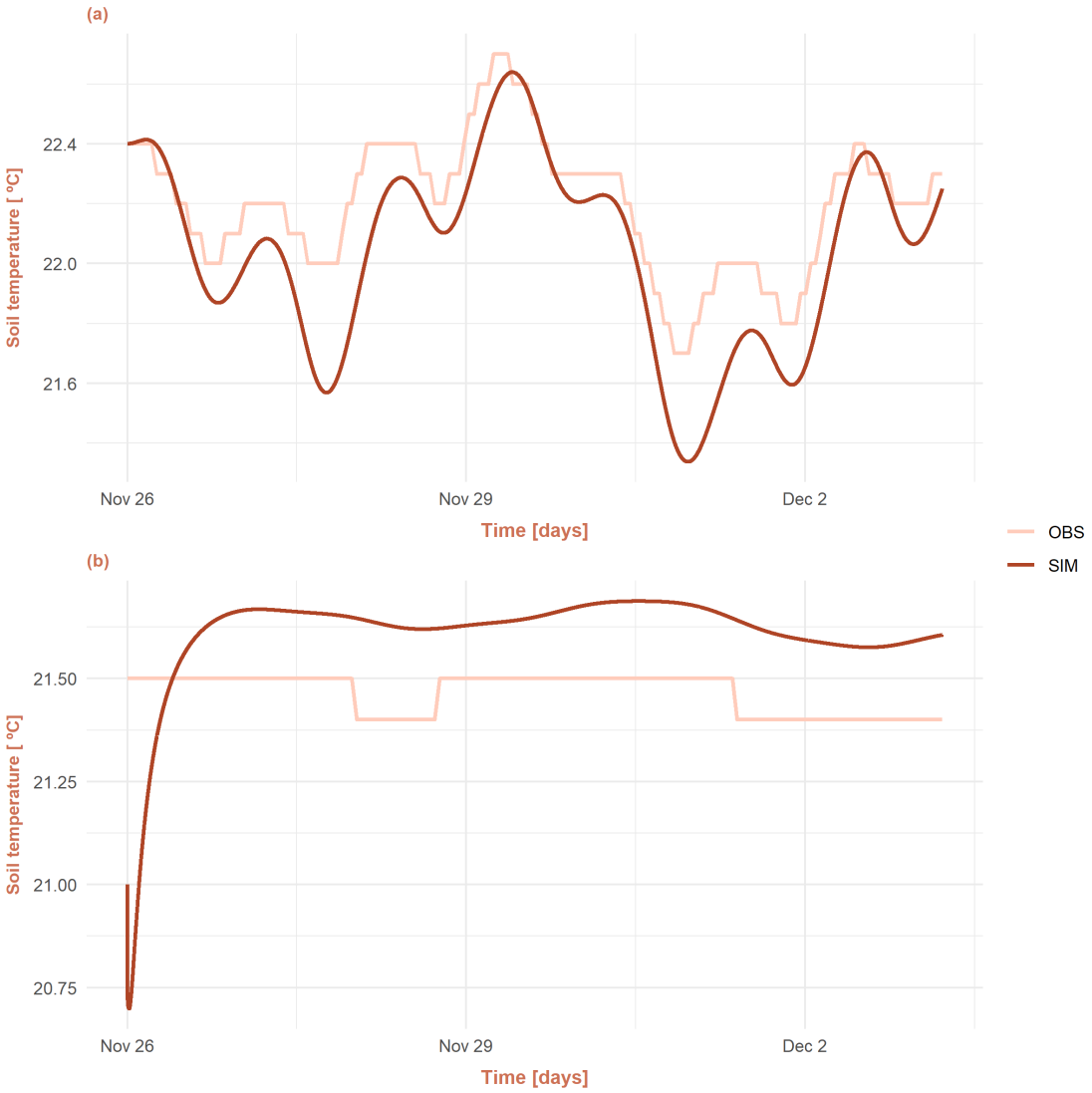

Figure 4.8: Simulated versus observed soil temperature at depths (a) 0.35 m and (b) 0.8 m during the validation scenario (16 Feb. 2021 - 22 Feb. 2021).

4.3 Sensitivity Analysis

To understand the effects of the saturated hydraulic conductivity on modelling evaporation in the soil, a sensitivity analysis of this parameter was conducted over the chosen calibration period. Figure 4.9 depicts simulated pressure head values at 0.35 and 0.8 m depths after decreasing K_s by 2 orders of magnitudes of the value initially chosen. It can be seen that the estimated pressure head at 0.8 m increases when decreasing the hydraulic conductivity, and thus the value of h is progressively overestimated in comparison to the measured values. On the other hand, a lower K_s had the opposite effect on h values at the depth of 0.35 m, i.e., it regularly decreased the estimation of pressure head. Moreover, when examining Figure 4.10 depicting the influence of hydraulic conductivity on

the soil temperature, the overestimation of the values of T with the lower K_s is evident at both depths.

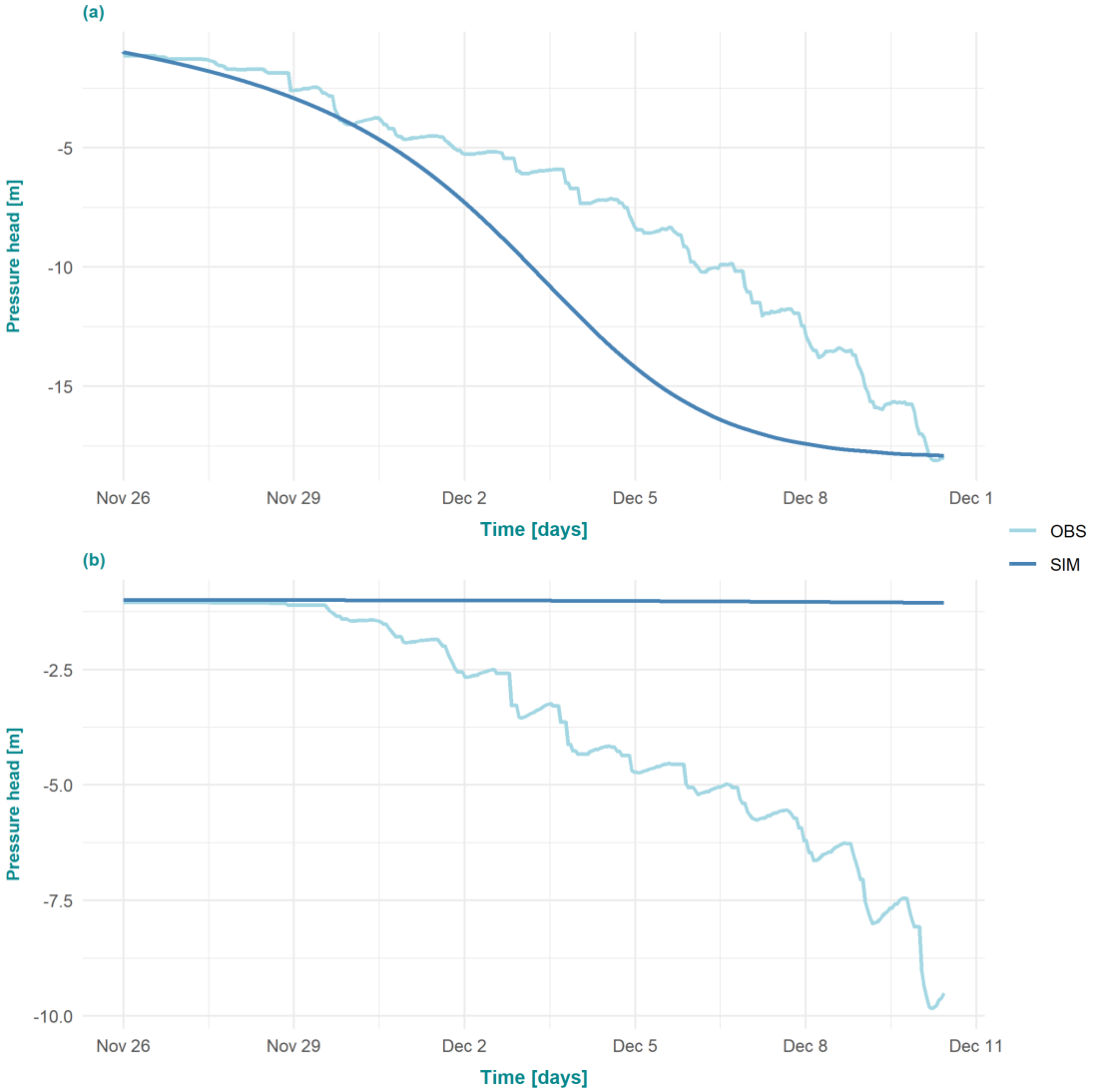

Figure 4.9: Saturated hydraulic conductivity effect on estimated pressure head, as a part of the sensitivity tests conducted on K_s.

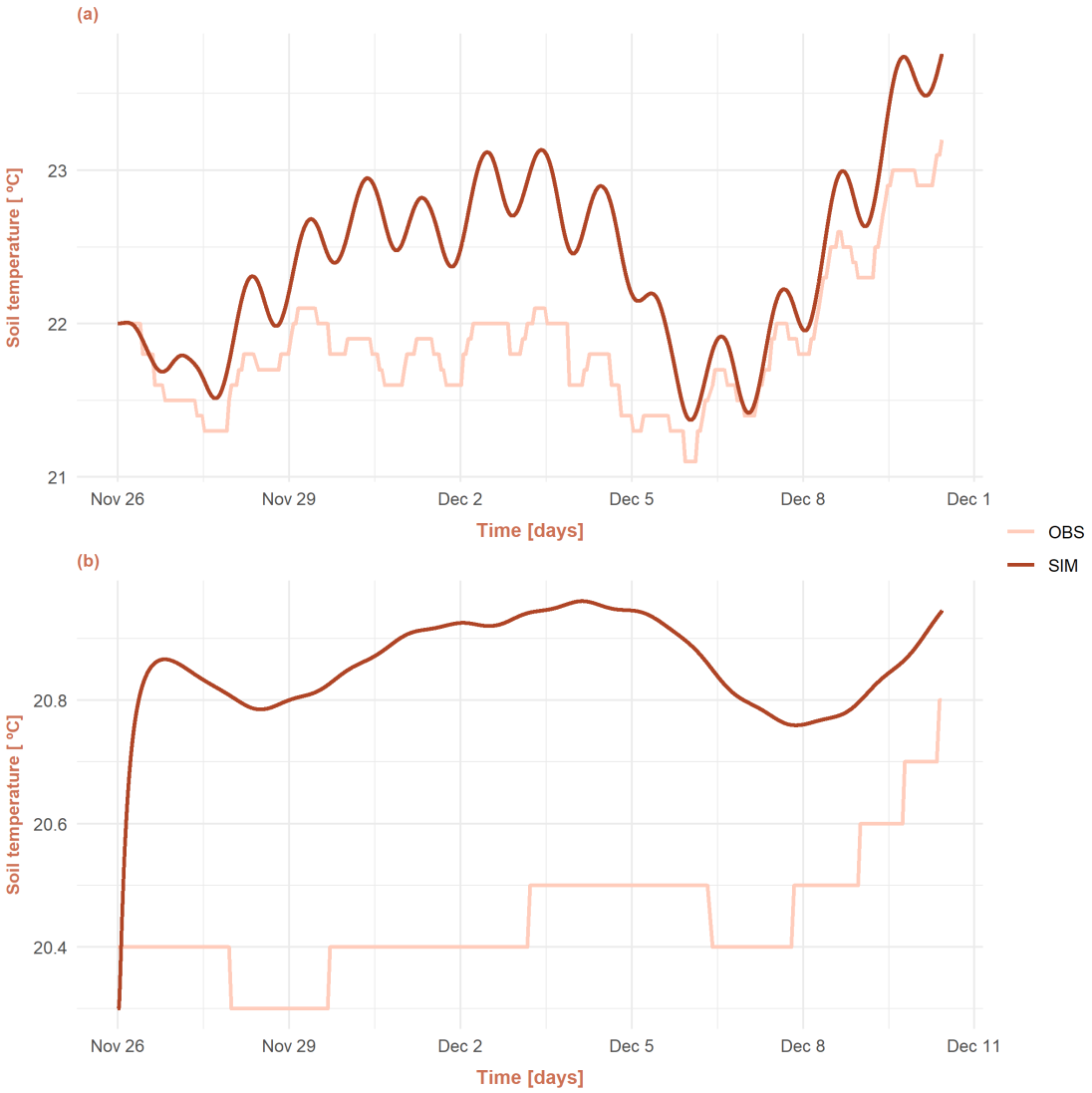

Figure 4.10: Saturated hydraulic conductivity effect on estimated soil temperature, as a part of the sensitivity tests conducted on K_s.

Chapter 5

Discussion

The model used in this thesis to investigate evaporation from porous media is complex. The number of parameters that require fine-tuning is large, which allows a great degree of freedom with regards to focus-versus-time-constraints choices. In this chapter, essential model parameters will be discussed, paired with the input-data assumptions involved and the technical aspects in the choices of this model.

5.1 Water Transport Model

5.1.1 Water retention capacity

Since soil retention water capacity is related to pore size distribution and defined as $C = d\theta/dh$, the effects of the inverse of air entry value α and the shape parameter n can be also reflected in the calculations of C. When values of the van Genuchten parameters produced by *Rosetta* were used in the simulation, the model output resulted in pressure-head that was lower than observations and soil temperature that was considerably higher. This might be due to different soil composition than the standard profiles considered in *Rosetta*. In the second calibration run, van Genuchten parameters were lowered, resulting in a better precision in terms of both pressure head and soil temperature at both 0.35 and 0.8 m depths.

5.1.2 Root water uptake

Simulations of pressure head generally displayed a lack of diurnal patterns. This lead to the consideration that changes to the soil water content due to root water uptake are not reflected properly. Water uptake from the roots was incorporated

in the model as a constant value at each of the 6 layers. However, it is possible that this term requires a more dynamic configuration. Values for the sink term matric potential heads and maximum plant transpiration were computed using Hydrus-1D (Jirka Simunek et al., 2005) for grapevines. Calculated S_{max} was higher than what was suitable for the study site profile, and assigning it to half the original used value corresponded with a better representation. This suggests that water uptake from plant roots may not be active at night, since a constant but lower value of maximum transpiration produced better simulation results. Although this was a better fit for the model, it does not describe physical reality properly. A possible more-accurate representation may include a root water uptake term that is turned off nightly.

5.2 Heat Transport Model

5.2.1 Heat capacities

In the first simulation, diurnal changes in pressure head values were not apparent at all. One possible reason for this might have been the decreasing intensity of the heat signal from the boundary condition as we progress from the surface to the deeper layers of the soil. The minor discrepancies in the final predictions of soil temperature could be due to a high value of soil heat capacity. Since the soil profile of the study site was not given with exact composition measures, assumptions had to be made according to the closest values in related literature. After the first simulation, original values from Kodešová et al. (2013) were altered by increasing the capacity of dry soil to account for the presence of organic roots in layers 4 and 5. Thermal conductivity parameters b_1 to b_3 are also factors in determining the speed with which heat gets transported. Due to lack of specific soil composition information, initial assumptions were made based on values introduced in Chung and Horton (1987) under the consideration of silt-dominance in the silty clay loam layer. In the second simulation this was changed to reflect clay-corresponding values which proved to be more consistent with physical reality as reflected in the temperature and pressure head plots of the final stage.

5.2.2 Air temperature

The effects of air temperature on the surface layer of the soil extends to the values of the sensible heat flux H. This is because H is calculated primarily from the difference between soil and air temperatures. Air temperature at the study site was not explicitly available, therefore its value was taken from the data of the

meteorological station, and assumed as equal to that of the station's location (roughly 9 km away from the city of San Juan). This could have played a role in the precision of the computations of the sensible heat flux. The value of air temperature also influences the evaporation rate, due to equation 2.60 where E is calculated from the difference between soil and air vapor pressure density. This difference is governed by air temperature, hence the possible inaccuracy of E's prediction. At the same time, the assumption of air temperature that is identical to that of the meteorological station does not take into account the presence of shade at the vineyard. This also gives way to a possible misrepresentation of the cloudiness of the atmosphere (i.e., the ratio of actual to maximum-possible sunshine duration n/N, which was assumed to be equal to 1 indicating a clear day). Although it is worth stating that due to the high averages of monthly sunshine hours in San Juan, this assumption may not have had a notable effect.

5.2.3 Resistance terms

While bare soil evaporation is already complex, modelling evaporation from vegetated soil is even more difficult. Many methods neglect the soil surface resistance term when modelling coupled water, vapor, and heat flows. However, it was included in this model's computation of the evaporation rate as a representation of the plants' roughness. The influence of a strong r_s term was detected in the early stages of simulation, where evaporation was overestimated possibly due to its high value. This was also a potential explanation for the increase in initial soil temperature simulated values once the water content threshold set for activating the resistance term was reached. Other factors that may have played a role in the soil surface resistance precision include the estimation of some plant-specific parameters, such as leaf area index (LAI) and stomatal conductance. Both of those parameter vary according to different growth periods of the plants.

On the other hand, aerodynamic resistance r_H could have introduced some problems as well. The model assumes that data from the meteorological station represents a height of 1.5 m above vine level. Since the height of plants factors in the heat and vapor momentum transfer in r_H, this could pose a misinterpretation in case of inaccurately assigned levels. That in turn, would translate poorly in terms of wind speed information, since wind changes according to different heights and above surfaces with different roughness.

All of the above suggests that acquiring exact measurements of LAI and plants' time-varying height would improve the soil surface resistance estimation greatly.

5.3 Technical Uncertainties

Due the lack of long-period data provided, the choice of calibration and validation periods was limited. Modelling evaporation with precision requires lengthy simulations to assert and account for the data uncertainties. In this research however, the chosen simulation intervals depended on data availability from two sources. Data from the national weather station was used to obtain the preliminary input parameters to the surface energy balance equation. After running the model, observations recorded at the soil sensors API were used for model output comparison. While the records of the meteorological station were mostly reliable, the same cannot be said of the soil sensor readings. Since some measurements were missing over certain interminable time-frames, choosing the simulation periods was constrained. This had a considerable impact on the model's ability to deal with data uncertainties. Another technical difficulty faced was the lack of accurate study-site irrigation schedules, which required a trial-and-error selection procedure to identify those events. Lastly, the apparent inconsistency of irrigation events (concluded from the observations of the soil water potential) also interfered with the period choice since the model does not include irrigation representation in combination with the surface energy balance.

Chapter 6

Conclusions and Recommendations

In this thesis, evaporation losses were investigated using the coupled liquid water, water vapor, and heat flow numerical model implemented in the open-source software DRUtES. The main aim of this study was to build a system of pressure head and soil temperature prediction. Python scripts were developed to automate the input to the surface energy balance equation as a part of the configuration of DRUtES. Observation record generation was also automated using a code programmed in Python, and later used to obtain estimates of the system's initial boundaries from in-situ sensor measurements. The surface energy balance equation solution was computed based on models suggested by Allen et al. (1998) and Monteith and Unsworth (2013). A case study was undertaken at a vineyard in San Juan, Argentina, in order to evaluate and validate the predictions of the model. Sensitivity tests were performed on the saturated hydraulic conductivity parameter to investigate its influence on the model's performance. The results of simulations measured well against the observed values obtained from the soil sensors. The model succeeded in characterizing the non-isothermal evaporation rate and produced accurate description of the pressure head and soil temperature. This can be used to facilitate efficient water-usage and optimize irrigation methods, thereby aiding the solution to soil saturation and increased salinity problems.

6.1 Future Research Recommendations

Due to technical difficulties associated with availability and reliability of meteorological and observation data sources, long-term simulations were not conducted.

However, the preliminary results pose interesting and important questions for future research. As a participation towards the AgriClima (2019) project, further development of the project could be achieved by the following essential suggestions:

- Dynamically implementing the root water uptake term, with regards to its time-dependant denotation.
- Including irrigation events representation combined with the surface energy balance as factors influencing the evaporation process.
- Exploring the effects of meteorological data instability on the accuracy of the model's prediction.
- Conducting sensitivity analysis on van Genuchten parameters α and n to determine their impact on the estimation of evaporation rate.
- Providing a complete soil hydraulic properties field description for more accurate simulation results and comparisons.
- Time-varying implementation of the soil surface resistance and aerodynamic resistance to reflect the diurnal changes of the soil water content.

6.2 Software Model Recommendations

With the aim of improving all aspects of the evaporation model implemented in DRUtES, the following points could be considered:

- Revising the pre-requirements of model execution that are placed on the configuration files. For instance, some values are obligatory to fill in the configuration files, despite the model actually calculating it from other values, or acquiring it elsewhere.
- Adjusting the configuration of the mesh generator to reflect the domain more clearly (e.g., descritizing the layers in a more typical soil-depth representation with the surface value assigned as 0 m depth) to avoid confusion.
- Including more explanatory comments for an enhanced user-friendly experience. For instance, some configurations had to be selected as numeric values (e.g., boundary type) without providing the meaning of each possible choice.

Bibliography

AgriClima (2019). *Adding Value through Piloting of the EU-CELAC Climate Services Market in Agriculture*. https://www.fzp.czu.cz/en/r-9411-projects-and-partnerships/r-9880-projects/r-14937-agriclima-adding-value-through-piloting-of-the-eu-celac-climate-services-market-in-agriculture. Online; accessed on 2020.

Allen, Richard G et al. (1998). "FAO Irrigation and drainage paper No. 56". In: *Rome: Food and Agriculture Organization of the United Nations* 56.97, e156.

Ångström, Anders (1929). "On the atmospheric transmission of sun radiation and on dust in the air". In: *Geografiska Annaler* 11.2, pp. 156–166.

Bittelli, Marco et al. (2008). "Coupling of heat, water vapor, and liquid water fluxes to compute evaporation in bare soils". In: *Journal of Hydrology* 362.3-4, pp. 191–205.

Brooks, Royal Harvard and Arthur Thomas Corey (1964). "Hydraulic properties of porous media". PhD thesis. Colorado State University. Libraries.

Brutsaert, Wilfried (2013). *Evaporation into the atmosphere: theory, history and applications*. Vol. 1. Springer Science & Business Media.

Burt, Charles M et al. (2005). "Evaporation research: Review and interpretation". In: *Journal of irrigation and drainage engineering* 131.1, pp. 37–58.

Cahill, Anthony T and Marc B Parlange (1998). "On water vapor transport in field soils". In: *Water Resources Research* 34.4, pp. 731–739.

Camillo, Peter J and Robert J Gurney (1986). "A resistance parameter for bare-soil evaporation models". In: *Soil Science* 141.2, pp. 95–105.

Chung, Sang-Ok and Robert Horton (1987). "Soil heat and water flow with a partial surface mulch". In: *Water Resources Research* 23.12, pp. 2175–2186.

Coakley, JA (2003). "Reflectance and albedo, surface". In: *Encyclopedia of the Atmosphere*, pp. 1914–1923.

De Vries, DA (1958). "Simultaneous transfer of heat and moisture in porous media". In: *Eos, Transactions American Geophysical Union* 39.5, pp. 909–916.

Feddes, RA, PJ Kowalik, and H Zaradny (1978). "Simulation of field water use and crop yield, Simul". In: *Monogr. PUDOC, Wageningen*.

Gardner, WR (1958). "Some steady-state solutions of the unsaturated moisture flow equation with application to evaporation from a water table". In: *Soil science* 85.4, pp. 228–232.

Han, Jiangbo and Zhifang Zhou (2013). "Dynamics of soil water evaporation during soil drying: laboratory experiment and numerical analysis". In: *The Scientific World Journal* 2013.

Iden, Sascha C et al. (2019). "Numerical test of the laboratory evaporation method using coupled water, vapor and heat flow modelling". In: *Journal of Hydrology* 570, pp. 574–583.

Kačur, J (2001). "Solution of nonlinear and degenerate convection–diffusion problems". In: *Nonlinear Analysis: Theory, Methods & Applications* 47.1, pp. 123–134.

Kodešová, Radka et al. (2013). "Thermal properties of representative soils of the Czech Republic". In: *Soil and Water Research* 8.4, pp. 141–150.

Kondo, Junsei, Nobuko Saigusa, and Takeshi Sato (1990). "A parameterization of evaporation from bare soil surfaces". In: *Journal of Applied Meteorology and Climatology* 29.5, pp. 385–389.

Kool, D et al. (2014). "Spatial and diurnal below canopy evaporation in a desert vineyard: Measurements and modeling". In: *Water Resources Research* 50.8, pp. 7035–7049.

Kuraz, Michal, Petr Mayer, and Johanna Ruth Blöcher (2020). *DRUtES – an opensource library for solving coupled nonlinear convection-diffusion-reaction equations*. URL: `http://www.drutes.org`.

Kuraz, Michal, Petr Mayer, and Pavel Pech (2014). "Solving the nonlinear Richards equation model with adaptive domain decomposition". In: *Journal of Computational and Applied Mathematics* 270, pp. 2–11.

Kuráž, Michal and Johanna R. Bloecher (2017). *Hydrodynamic of porous media*. Teaching notes. Prague, Czech Republic: Faculty of Environmental Sciences, Czech University of Life Sciences Prague.

Ltd (2021). *LESPROJEKT-SLUŽBY s.r.o company*. `https://www.lesprojekt.cz/`. Online.

McMahon, TA et al. (2013). "Estimating actual, potential, reference crop and pan evaporation using standard meteorological data: a pragmatic synthesis". In: *Hydrology and Earth System Sciences* 17.4, pp. 1331–1363.

Millington, RJ and JP Quirk (1961). "Permeability of porous solids". In: *Transactions of the Faraday Society* 57, pp. 1200–1207.

Monteith, John and Mike Unsworth (2013). *Principles of environmental physics: plants, animals, and the atmosphere*. Academic Press.

Mualem, Yechezkel (1976). "A new model for predicting the hydraulic conductivity of unsaturated porous media". In: *Water resources research* 12.3, pp. 513–522.

Nassar, IN and Robert Horton (1997). "Heat, water, and solution transfer in unsaturated porous media: I–theory development and transport coefficient evaluation". In: *Transport in porous media* 27.1, pp. 17–38.

Nimmo, JR and EE Miller (1986). "The temperature dependence of isothermal moisture vs. potential characteristics of soils". In: *Soil Science Society of America Journal* 50.5, pp. 1105–1113.

Noborio, K., K. J. McInnes, and J. L. Heilman (1996). "Two-dimensional model for water, heat, and solute transport in furrow-irrigated soil: I. Theory". In: *Soil Science Society of America Journal* 60.4, pp. 1001–1009.

Noborio, Kosuke, KJ McInnes, and JL Heilman (1996). "Two-dimensional model for water, heat, and solute transport in furrow-irrigated soil: II. Field evaluation". In: *Soil Science Society of America Journal* 60.4, pp. 1010–1021.

Or, Dani et al. (2013). "Advances in soil evaporation physics—A review". In: *Vadose Zone Journal* 12.4, pp. 1–16.

Peters, Andre, Wolfgang Durner, and Sascha C Iden (2017). "Modified Feddes type stress reduction function for modeling root water uptake: Accounting for limited aeration and low water potential". In: *Agricultural Water Management* 185, pp. 126–136.

Philip, JR and DA De Vries (1957). "Moisture movement in porous materials under temperature gradients". In: *Eos, Transactions American Geophysical Union* 38.2, pp. 222–232.

Richards, Lorenzo Adolph (1931). "Capillary conduction of liquids through porous mediums". In: *Physics* 1.5, pp. 318–333.

Ritchie, Joe T (1972). "Model for predicting evaporation from a row crop with incomplete cover". In: *Water resources research* 8.5, pp. 1204–1213.

Saito, Hirotaka, Jiri Šimůnek, and Binayak P Mohanty (2006). "Numerical analysis of coupled water, vapor, and heat transport in the vadose zone". In: *Vadose Zone Journal* 5.2, pp. 784–800.

Sakai, Masaru, Scott B Jones, and Markus Tuller (2011). "Numerical evaluation of subsurface soil water evaporation derived from sensible heat balance". In: *Water Resources Research* 47.2.

Schaap, Marcel G, Feike J Leij, and Martinus Th Van Genuchten (2001). "Rosetta: A computer program for estimating soil hydraulic parameters with hierarchical pedotransfer functions". In: *Journal of hydrology* 251.3-4, pp. 163–176.

Shahid, Shabbir A, Mohammad Zaman, and Lee Heng (2018). "Salinity and sodicity adaptation and mitigation options". In: *Guideline for salinity assessment, mitigation and adaptation using nuclear and related techniques*. Springer, pp. 55–89.

Simunek, J and DL Suarez (1993). "UNSATCHEM-2D code for simulating two-dimensional variably saturated water flow, heat transport, carbon dioxide production and transport, and multicomponent solute transport with major ion equilibrium and kinetic chemistry". In: *Agricultural Research Service, US Department of Agriculture, Riverside, California*.

Simunek, Jirka, M Th Van Genuchten, and M Sejna (2005). "The HYDRUS-1D software package for simulating the one-dimensional movement of wa-

ter, heat, and multiple solutes in variably-saturated media". In: *University of California-Riverside Research Reports* 3, pp. 1–240.

SMN (2020). *Servicio Meteorológico Nacional*. `https://www.smn.gob.ar/descarga-de-datos`. Online; accessed 'datos meteorológicos horarios'.

Tezza, Luca et al. (2019). "Measuring and Modelling Soil Evaporation in an Irrigated Olive Orchard to Improve Water Management". In: *Water* 11.12, p. 2529.

Van Bavel, CHM and DI Hillel (1976). "Calculating potential and actual evaporation from a bare soil surface by simulation of concurrent flow of water and heat". In: *Agricultural Meteorology* 17.6, pp. 453–476.

Van Genuchten, M Th (1980). "A closed-form equation for predicting the hydraulic conductivity of unsaturated soils". In: *Soil science society of America journal* 44.5, pp. 892–898.

Vanderborght, Jan et al. (2017). "Heat and water transport in soils and across the soil-atmosphere interface: 1. Theory and different model concepts". In: *Water Resources Research* 53.2, pp. 1057–1079.